POLITECNICO DI TORINO

NANOTECHNOLOGIES FOR ICTS

MASTER DEGREE THESIS

Nanoporous membranes as a filter for SERS detection

October 2018

Thierry FERRERO

Relatore:

Prof. Carlo RICCIARDI

A.A 2017/2018

Acknowledgments

I would first like to thank my thesis advisor Carlo Ricciardi, professor of Politecnico di Torino for having supported my internship project and helped me during the work's organization. He consistently allowed this paper to be my own work, but steered me in the right the direction whenever he thought I needed it.

I would also like to thank a lot the experts that followed my work in the laboratory in Paris and gave me the possibility of joining their projects:

- Nathalie Lidgi-Guigui, "maître de conférences" among Université Paris 13;
- Giulia Fadda, "maître de conférences" among Université Paris 13 and researcher at LLB (Laboratoire Leon Brillouin) of CEA France;
- Didier Lairez, researcher at LSI (Laboratoire des Solides Irradiés) in Ecole Polytechnique.

They helped me during the practical work and always gave me advices based on their knowledge and experience, I must express my very profound gratitude for all what I have acquired from them; I really feel having learned a lot.

I would like to thank my parents and my brothers for their constant support despite the distance; a special thanksgiving to my parents for their continuous encouragement and efforts to sustain this possibility that I had.

Another special mention goes to my friends, always ready to warmingly welcome me back home and for having always exploited my stay away like a possibility to improve the friendship and meeting in a unusual way.

Last but not the least, I would like to thank Carola for all the constant and strong support given during the time abroad, helping me every moment of the year in every life situation. The distance has become a different way to stay close with her.

During this year I met so many people in different situations that made me aware how the world is amazing and diversified. Every person I stayed with, it doesn't care if for a few minutes or for some months, must receive a great thanks from me.
I never felt alone for an instance, for this reason I want to end with a very special sentence:

"Happiness is real only when shared", Christopher McCandless.

Contents

1 Introduction

The purpose of the project is to gather two very different techniques for a better biomolecular sensing.
The first side consists in developing a sensor for Surface Enhanced Raman Spectroscopy (SERS) in order to detect the proteins exploiting the high signal coming from the plasmonic effect of gold nanoparticles. Here the work would be the evaluation of different kinds of substrates in order to compare their behavior and characterize the best procedure for the proteins detection.
The second technique is based on the utilization of nanoporous membranes for liquid filtration. The basic principle would be to increase the concentration of a targeted molecule in order to facilitate the SERS detection. This work started from the beginning, so from the basic building and optimization of the device until studying the membranes behavior with polymers.
These two subjects are carried out in parallel in two different laboratories, the internship consisted in working in both places in order to make progress simultaneously on the two projects.
The involved laboratories are:

- LSI (Laboratoire des Solides Irradiés) at the Ecole Polytechnique in Palaiseau.

(a) Ecole Polytechnique - Palaiseau

(b) LSI elettro-chemical lab

- CSPBAT (Chimie, Structures, Propriétés de Biomatériaux et d'Agents Thérapeutiques), UMR CNRS 7244 int Université Paris 13 at Bobigny;

(a) Université Paris 13 - Bobigny

(b) CSPBAT preparation lab

The first laboratory is the one used for the study on the membrane and its preparation; in the second one is carried out development of the biosensor and the proteins processes.

My supervisors during the work were:

- Nathalie Lidgi-Guigui, "maître de conférences" in Bobigny, she was helping me with the sensing part;
- Giulia Fadda, "maître de conférences" in Bobigny and researcher among LLB (Laboratoire Leon Brillouin) at CEA (Commissariat á l'énergie atomique et aux énergies alternatives). She was following me in Ecole Polytechnique concerning the filtration with the membrane.

During my internship and my time in Polytechnique I worked also with Didier Lairez, researcher among LSI (Laboratoire des Solides Irradiés); he helped me in the electrical measurements on the membrane and in the part concerning the theoretical investigation.

1.1 Biosensors

Biosensors are analytical devices that transduce a biological effect into an electric signal; they are used to detect the presence of a specific biomolecule, a precise structure or a microorganism. Often their aim consists in producing an electronic signal that is proportional to the concentration of a specific analyte [1].

These devices are mainly composed by three parts:

- a component that recognizes the analyte and produces a signal;
- a signal transducer;
- a reader device for the response.

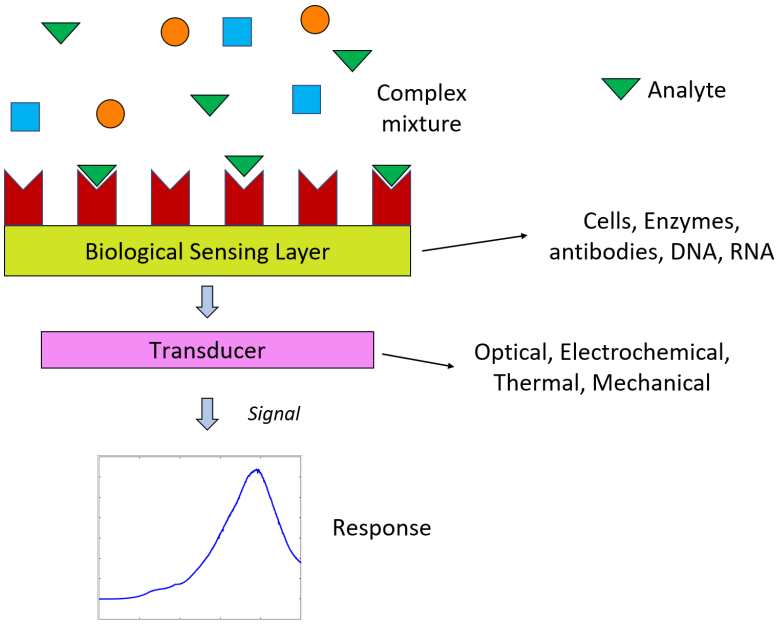

Figure 3: Working scheme for a biosensor.

The most crucial part of the device is the transducer, whose aim is to transform one signal in another one and it can act following different physicochemical ways: optical, electrochemical, thermal, electrochemical, mechanical etc. In particular these phenomena are coming from the interaction between the sample and the bio-element.
The devices are connected with the electronics and the signal processors, finally a display gives the result.

The most important properties for a biosensor are the specificity and the sensitivity; the first one is the ability to react to a specific element and be, as much as possible, non-reactive to other species. For this purpose it should be able to identify a specific component in a heterogeneous sample.
The sensitivity represents the minimum amount of quantity (or concentration) that is possible to detect with the sensor, obviously it should be as lower as possible.

The development of biosensors is coming from different fronts; new possible approaches are always proposed, as well as novel engineering components and biochemical reactions[2].

The main applications related to the biosensing field are[3]:

- Food analysis;
- Study of Biomolecules and their interactions;
- Drug development, crime detection;
- Medical diagnosis;
- Environmental field monitoring;
- Industrial process control;
- Manufacturing of pharmaceuticals and replacement of organs.

There are many possible combinations between the sensing element and the transducer, making this kind of field very multidisciplinary[3]. In fact the development of such a system comes from the investigation of many aspects, starting from the pure biological activity until the engineering of the devices and the electronics of the components, passing through immobilization techniques.
In the last years they faced a huge growth due to the increased interest in biotechnology for many different applications.

In our case we will deal with sensor based on the Surface Enhanced Raman Spectroscopy (SERS) technique[4].
They had a very huge development in the past decade and a lot of improvements concerning the sensitivity and the detection limit are currently ongoing[5].
In this case the big sensitivity enhancement comes from the increased overlap integral of the electromagnetic field at the interface between the substrate and the biomolecule.

2 Theory

2.1 Surface Enhanced Raman Spectroscopy

Spectroscopy is the study of the interaction between electromagnetic radiation and matter.
At the beginning this term was associated to the study of light dispersion, as for the wavelength experiment of the prism.
Afterwards the word assumed a broadened meaning, referring to any interaction of radiative energy that permits to obtain a response as a function of wavelength (or frequency).

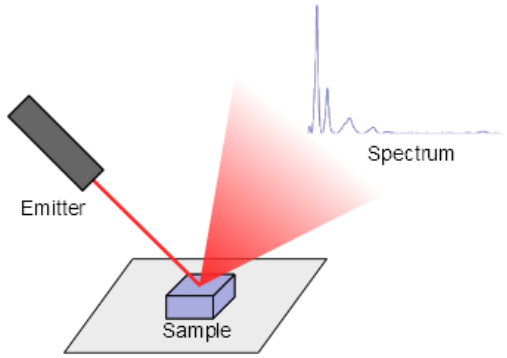

Figure 4: Basic principle of spectroscopy, from
http://www-anw.cs.umass.edu/legacy/spectroscopy.shtml

There are different kinds of spectroscopy, they strictly depend on the nature of the involved interaction. The most common are[6]:

- *Elastic scattering and reflection spectroscopy*: it can be used to get informations about reflection or scattering of the incoming radiation[7]. The main application comes from the crystallography, that uses the scattering of X-rays or electrons to characterize the atomic configurations in crystals and proteins;
- *Absorption*: in this case the incoming radiation is absorbed by the sample[8]. It can be obtained looking at the transmission through the material;
- *Emission*: here the energy is released by the sample. It can be spontaneous, like in the case of the blackbody radiation of a material, or stimulated by any incoming flux, like in the case of fluorescence[9];
- *Inelastic scattering*: in this case there is an exchange of energy between the incoming flux and the sample, leading to a variation in energy of the radiation that gives informations about the material. The most famous example is the Raman effect;
- *Impedance*: this effect is related to the property of a medium of slowing the transmittance of the radiation, linked to the refraction index of the material[10];
- *Coherence*: this is based on the coupling between a radiation and the quantum states of the sample. A big example is the NMR (Nuclear Magnetic Resonance) spectroscopy[11].

In our case we will deal Surface Enhanced Raman Spectroscopy, a technique based on the inelastic scattering between light and a medium.

2.1.1 Raman Theory

Raman spectroscopy is a versatile method for the analysis of a huge range of different samples; the main advantage of this technique is the possibility of performing both qualitative and quantitative measurements, looking at the scattered radiations in the first case and at their intensity for the second.

The basic principle is the following: when a monochromatic radiation of a certain frequency impinges on a sample composed by molecules or crystals, most of the flux is transmitted without any change in energy (and so wavelength); however a small fraction of the light will be scattered leading to a variation of the wavelength (and energy).

Energy and wavelength are directly related by the Planck's formula:

$$E = h \cdot \nu = h \cdot \frac{c}{\lambda} \tag{1}$$

where h is the Planck constant, ν is the frequency and λ is the wavelength.

The part of the light that is not scattered follows the elastic process (no energy variation) and it's called the Rayleigh scattering.
The inelastic process (so when scattering happens leading to an energy variation of photons) is called the Raman effect.

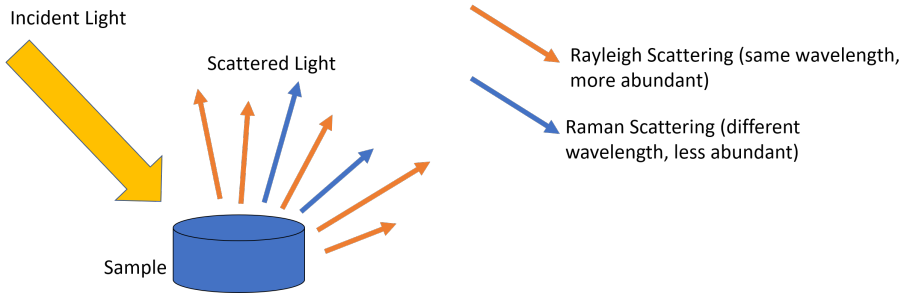

Figure 5: Basics of scattering interactions.

The Raman process was discovered in 1928 by the Indian professor Chandrashekhara Venkata Raman who got the Physics Nobel prize in 1930[12].

The explained interaction happens between the photon flux and the electric dipole of the molecules[13].
Looking at the energy variations it's possible to get the typical frequencies associated to transitions between rotational, vibrational and electronic levels; these frequencies are called normal modes and they are related to different types of motion and symmetry.
The output spectrum is built measuring the shift in energy with respect to the incoming radiation, getting peaks related to the energies of molecular vibrations. In the typical representation the shift is indicated with the wavenumber k, that it related to the wavelength with:

$$k = \frac{2\pi}{\lambda} \tag{2}$$

The final spectrum will be the collected intensity as a function of the wavenumber.

From a general point of view, we can consider an incoming flux of n_1 photons with energy $\hbar\omega_1$ on a molecule with energy E_i.
The interaction of one photon will bring the molecule to the energy E_f and the photon will go out with energy $\hbar\omega_2$.
Then the difference $E = \hbar\omega_1 - \hbar\omega_2$ represents the energy of a jump between two possible states of the molecule.
In this case the outgoing photon will be characterized by a lower energy, that means lower frequency (see Eq. 1).
This kind of interaction is called Stokes scattering (see figure 6).

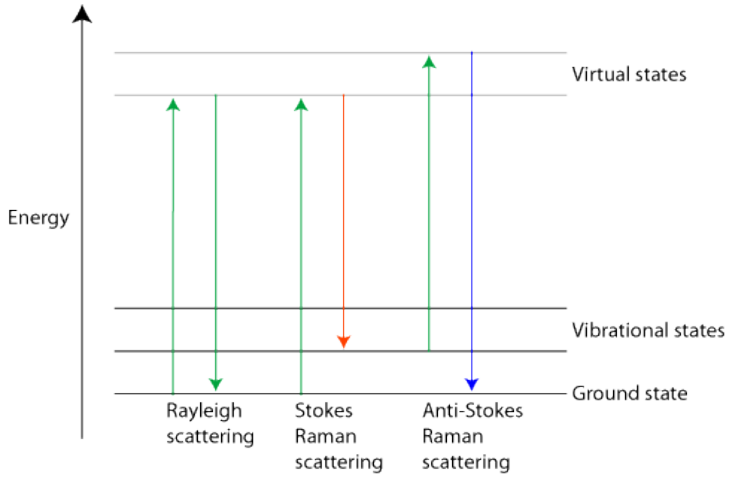

Figure 6: Vibrational transition in Raman spectroscopy, from https://www.doitpoms.ac.uk/tlplib/raman/raman_scattering.php.

In the opposite case the molecule is going from an excited state to a lower one, the outgoing photons will be characterized by higher energy with respect to the incoming ones and this phenomenon is called the anti-Stokes effect.

At room temperature, most of the molecules contained in the sample are in the ground state, so the probability of an anti-Stokes scattering is much lower than a Stokes one.
This is the reason why the usual spectrometers are considering just the Stokes shifted light.

Classical point of view

On the classical side, light can be described as an electromagnetic radiation, with electric and magnetic fields oscillating at a certain frequency.
This radiation can interact with molecules through their polarizability and investigating this theory it's possible to give an explanation of scattering events, i.e. understand the interaction between the photons and the electric dipoles of molecules[14][15][16][17].

So let's consider the general case of an electrical dipole induced by an electric field, it can be written exploiting the power series[14]:

$$\mu = \mu^{(1)} + \mu^{(2)} + \mu^{(3)} + ... \tag{3}$$

And the terms can be expressed as:

$$\mu^{(1)} = \alpha \cdot E \tag{4}$$

where α is the polarizability sensor, so the linear response to an electric field E.

The higher order terms can be considered as:

$$\mu^{(2)} = \frac{1}{2}\beta \cdot EE \tag{5}$$

$$\mu^{(3)} = \frac{1}{6}\gamma \cdot EEE \tag{6}$$

but they can be neglected in the case of not very high electric field, like usually the case of Raman scattering[14].

The next step is to consider the interaction between a molecule and an electric field with harmonic oscillations at the frequancy ω_0.
If we just investigate the vibrational modes, the polarizability tensor takes the form:

$$\alpha_{ij} = (\alpha_{ij})_0 + \sum_k \left(\frac{\partial \alpha_{ij}}{\partial Q_k}\right)_0 Q_k + \frac{1}{2}\sum_{k,l}\left(\frac{\partial^2 \alpha_{ij}}{\partial Q_k \partial Q_l}\right)_0 Q_k Q_l + ... \tag{7}$$

here the $(\alpha_{ij})_0$ represents the quantity at the equilibrium and Q_k, Q_l are the vibrational normal modes of the molecule with the relative frequencies ω_k, ω_l.

In the harmonic approximation we can neglect all the terms after the first order, leading to:

$$\alpha_{ij} = (\alpha_{ij})_0 + \left(\frac{\partial \alpha_{ij}}{\partial Q_k}\right)_0 Q_k \tag{8}$$

And for an harmonic vibration:

$$Q_k = Q_{k0}\cos(\omega_k t + \delta_k) \tag{9}$$

Finally considering the k vibration term and combining Eq. 8 and Eq. 9, the polarizability becomes:

$$\alpha_k = \alpha_0 + \left(\frac{\partial \alpha_k}{\partial Q_k}\right)_0 Q_{k0}\cos(\omega_k t + \delta_k) \tag{10}$$

Obtained this result, the first approximation of the electric dipole moment (under the effect of a radiation with frequency ω_0) is:

$$\begin{aligned}
\mu^{(1)} \quad &= \alpha_k \cdot E_0 \cos(\omega_0 t) = \\
&\alpha_0 \cdot E_0 \cos(\omega_0 t) + \left(\tfrac{\partial \alpha_k}{\partial Q_k}\right)_0 E_0 Q_{k0} \cos(\omega_0 t)\cos(\omega_k t + \delta_k) \cdot t = \\
&\alpha_0 \cdot E_0 \cos(\omega_0 t) + \tfrac{1}{2}\left(\tfrac{\partial \alpha_k}{\partial Q_k}\right)_0 E_0 Q_{k0} \cos(\omega_0 t + \omega_k t + \delta_k) + \tfrac{1}{2}\left(\tfrac{\partial \alpha_k}{\partial Q_k}\right)_0 E_0 Q_{k0} \cos(\omega_0 t - \omega_k t - \delta_k)
\end{aligned} \tag{11}$$

As we can notice, the final formula contains three terms:

- $\alpha_0 \cdot E_0 \cos(\omega_0 t)$ accounts for the Rayleigh scattering;
- $\frac{1}{2}\left(\frac{\partial \alpha_k}{\partial Q_k}\right)_0 E_0 Q_{k0} \cos(\omega_0 t + \omega_k t + \delta_k)$ accounts for the anti-Stokes Raman scattering $(\omega_0 + \omega_k)$;
- $\frac{1}{2}\left(\frac{\partial \alpha_k}{\partial Q_k}\right)_0 E_0 Q_{k0} \cos(\omega_0 t - \omega_k t - \delta_k)$ accounts for the Stokes Raman scattering $(\omega_0 - \omega_k)$.

So here is explained the mathematics of Rayleigh and Raman scatterings[14].
The Rayleigh event comes from the dipole oscillations at ω_0 induced in the molecule from the electric field of radiation at ω_0; differently the Raman scattering comes from the dipole moment oscillations at $\omega_0 \pm \omega_k$ due to the interaction between dipole moment at ω_0 (electric field) and vibrations at ω_k (molecule).

Quantum mechanical point of view

In the quantum picture a system can absorb or emit a radiation leading to a transition upwards or downwards between available energy levels[14][18][19] .
So the radiation and the molecule are considered as a unique complex system and studying their interaction it's possible to understand the energy exchange[14].
The transition moment can be defined using the Dirac notation as:

$$M_{f,i} = \langle \Psi_f | \mu | \Psi_i \rangle \tag{12}$$

where μ is the dipole moment operator and Ψ_i and Ψ_f are the wavefunctions of the initial and final states.

As explained in Eq.4 the electric dipole can be approximated to:

$$\mu^{(1)} = \alpha \cdot E \tag{13}$$

And so the transition moment becomes:

$$\mu^{(1)}{}_{f,i} = \langle \Psi_f | \alpha | \Psi_i \rangle \cdot E \tag{14}$$

Considering another time just the vibrational part, the matrix element of the polarizability tensor is given by:

$$[\alpha_{x,y}]_{f,i} = \langle \Phi_f | \alpha_{x,y} | \Phi_i \rangle \tag{15}$$

where Φ is the vibrational wavefunction.

Taking the same equation 7 of the classical theory but using a quantum notation and considering just the first order term:

$$[\alpha_{x,y}]_{f,i} = (\alpha_{x,y})_0 \langle \Phi_f | \Phi_i \rangle + \sum_k \left(\frac{\partial \alpha_{x,y}}{\partial Q_k}\right)_0 \langle \Phi_f | Q_k | \Phi_i \rangle \tag{16}$$

Then, working in the harmonic oscillator model, the total vibrational wavefunction corresponds to the product of the harmonic oscillator wavefunctions for every vibrational normal mode, so:

$$\Phi_i = \prod_k \Phi_{v_k^i}(Q_k) \tag{17}$$

where $\Phi_{v_k^i}(Q_k)$ is the harmonic wavefunction related to the normal coordinates Q_k, with a vibrational quantum number v_k^i.

For the harmonic oscillator functions, we can write:

$$\langle \Phi_{v_k^f}(Q_k) | \Phi_{v_k^f}(Q_k) \rangle = \begin{cases} 0 & \text{for } v_k^f \neq v_k^i \\ 1 & \text{for } v_k^f = v_k^i \end{cases} \tag{18}$$

that is related with the zero-order term

And:

$$\langle \Phi_{v_k^f}(Q_k) | Q_k | \Phi_{v_k^f}(Q_k) \rangle = \begin{cases} 0 & \text{for } v_k^f = v_k^i \\ (v_k^i + 1)^{\frac{1}{2}} b_{v_k} & \text{for } v_k^f = v_k^i + 1 \\ (v_k^i)^{\frac{1}{2}} b_{v_k} & \text{for } v_k^f = v_k^i - 1 \end{cases} \tag{19}$$

concerning the first-order term, with $b_{v_k} = \sqrt{\frac{h}{8\pi^2 v_k}}$

Selection rules

Now it's possible to find the condition at which the transition moment is different from zero[14][19].

Starting from the zero order term that represent the case of Rayleigh interaction (Eq. 18), the transition is non-zero when the condition $v_k^f = v_k^i$ is satisfied.
Examining the condition, it means that the vibrational quantum numbers doesn't change during the transition between the two states, that is exactly the case of Rayleigh scattering.

Looking at the Raman term (Eq. 19), taking the k-th therm as the referent transition, it should be non-zero and all the other terms should be zero.
So the vibrational quantum numbers must be conserved $v_j^f = v_j^i$ for the case $j \neq k$. In the k-th term the number should change of one unit (look at Eq. 19), so $v_k^f = v_k^i \pm 1$.
Analyzing the case, the transition associated to the momentum variation $\Delta v_k = +1$ is related with the Stokes scattering, while the case $\Delta v_k = -1$ stands for the anti-Stokes event.

From these conditions we can see that, in the harmonic approximation, only the transitions whose quantum number variations is by one unit are admitted in the Raman scattering; in particular, at least one element of the polarizability tensor must be non-zero.
From a more detailed analysis of the group theory, the elements of the tensor are non-zero only if they are characterized by the same symmetry with the second order terms, so x^2, y^2, z^2, xy, xz, yz. It means that a vibrational mode must have a basis in x^2, y^2, z^2, xy, xyz, yz [14].

Considering finally the vibrational transition polarizability elements, the fundamental transitions are described with:

$$[\alpha_{x,y}]_{f,i} = \langle \Phi_1 | \alpha_{x,y} | \Phi_0 \rangle \tag{20}$$

In these cases the initial state is characterized by all zero quantum numbers and in the final one only the k-th term has changed to one.
The integral in the Eq. 20 will be different from zero only in the case that $\alpha_{x,y}$ and $\Phi_1(Q_k)$ belong to equal symmetry species. It follows that they are evolving in the same way after a symmetry operation, this creates a selection rule for the Raman events related to fundamental transitions.

Generally, referring to all the possible transitions, we can finally say: a transition between two states, characterized by wavefunctions ψ_i and ψ_f is forbidden for Raman except if at least one of the triple products of the type $\psi_i \alpha_{x,y} \psi_f$ belongs to a representation whose structure contains the totally symmetric species.

In the figure 7 is shown the main idea of a Raman spectrometer and how the light is collected in order to build the final spectrum.

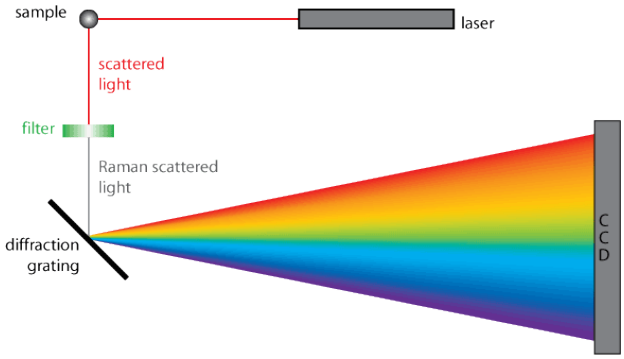

Figure 7: Basic configuration of a Raman spectrometer, from https://www.doitpoms.ac.uk/tlplib/raman/printall.php.

The utilization of a laser (monochromatic source) as a excitation is strictly needed due to the basic principle of Raman spectroscopy that consists in measuring the wavelength shift.
A further needed characteristic is the stability in frequency of the laser and a narrow bandwidth in order to get the sharpest possible Raman peaks.

This technique is really sample-dependent, i.e. the performance strongly depends on the chemical characteristics of the sample[20].
Every molecule is characterized by its "degrees of freedom", the total number of coordinates needed to describe it and its movements in the three-dimensional space; this number can be computed from N that is the number of nuclei present in the molecule [19][21].
The characterizing numbers can come from different effect, usually they are:

- *Translational Degrees of Freedom:* 3 coordinates are needed to describe the translational motion of the center of mass;
- *Rotational Degrees of Freedom:* 3 coordinates for describing the rotational motion in non-linear molecules; for linear molecules just 2 coordinates are sufficient;
- *Vibrational Degrees of Freedom:* the remaining coordinates are used to describe vibrational motion; in the case of non-linear molecule, the vibrational degrees are 3N - 6 while for a linear one they are 3N - 5 degrees.

	Total DoF	Translational DoF	Rotational DoF	Vibrational DoF
non-linear molecule	3N	3	3	3N - 6
linear molecule	3N	3	2	3N - 5

Table 1: Degrees of Freedom.

A linear molecule is characterized by a geometry developed around a central atom, with two atoms bonded with it and separated by 180° [22].

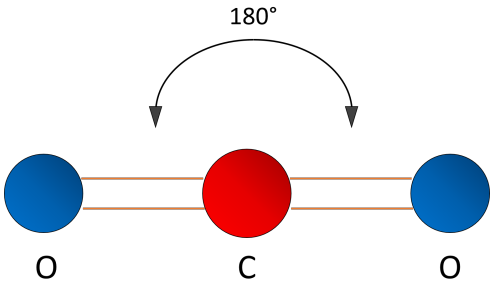

Figure 8: Linear Geometry example, CO_2 molecule.

Taking the example of the CO_2 [21], it contains 3 nuclei (N=3), so the total degrees of freedom are 3N=9.From these:

- 3 are translational;
- 2 are rotational;
- 3N-5 = 4 are vibrational.

The molecules characterized by a different geometry are non-linear and the degrees of freedom will follow the rules indicated in the table 1.

For each molecule it's possible to define the Raman cross-section, a parameter related to the polarizability of the molecule itself.
Moreover it can be defined as the ratio between the power at the detector P_S (so related to the scattered radiation) and the intensity incident on the sample I_0:

$$\sigma_R = \frac{P_S}{I_0} \tag{21}$$

It can be shown that the cross-section is inversely proportional to the incoming wavelength to the fourth power as:

$$\sigma_R \propto \frac{1}{\lambda^4} \tag{22}$$

And so finally:

$$P_S \propto \frac{I_0}{\lambda^4} \tag{23}$$

From this last equation we can notice the linearity between the power of the scattered light and the intensity of the incoming flux and the relationship with the inverse of the wavelength to the fourth power.

Therefore, it can be thought that the best condition is to work with the highest possible power and to use low excitation wavelength.
Anyway there is a trade-off between the characteristics: too much power can often damage the sample.

Concerning the laser wavelength, it is an important choice regarding the Raman technique: looking at the formula, it seems clear that shorter the wavelength, higher is the Raman signal. However this is not the only consideration especially when dealing with organic molecules; in fact most of them are affected by fluorescence when excited by high energy (short wavelength) photons, leading to the total invisibility of the Raman spectrum.

Exploiting Raman spectroscopy it's possible to create a fingerprint of a specific molecule, making this technique very suitable for the detection of particular elements in a heterogeneous sample.
The other important advantages of Raman are that it works in the visible range, it's quite easy to be implemented and finally it doesn't damage the sample.

The main drawback that should be often overcome is its poor sensitivity requiring a quite highly concentrated sample in order to be able to detect the particular component.
Due to this reason a way to enhance the output signal and the effect itself should be found: the easier and best way is to switch to SERS (Surface Enhanced Raman Spectroscopy) exploiting the high signal coming form the Localized Surface Plasmons.

2.1.2 Localized Surface Plasmons

Plasmonic effects are becoming more and more important in new technologies, their powerful properties can be exploited in a very huge range of applications [23][24].

The Surface Plasmon Resonance is a quantum effect that comes from the interaction between light and free electrons oscillating in a conductor-dielectric interface, more generally at the interface of negative and positive permittivity materials.
The resonant condition corresponds to the case of maximum coupling between the excitation flux and the surface, in this situation the energy carried by the photons is transferred to the interface electrons oscillations leading to collective excitations that are called Surface Plasmons (SPs).

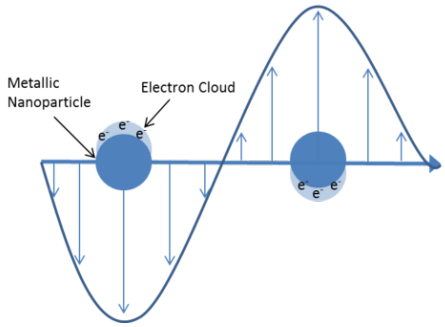

Figure 9: Plasmonic oscillations of metal nanoparticles in a dielectric environment. From the website https://nanohybrids.net/pages/plasmonics

This phenomenon is developed at the interface, where the field it's very strong while it decades exponentially with the distance perpendicular to it.
More precisely plasmons waves are confined at the interface with a penetration depth around 10-50 nm in the metal and 100-200 nm in the dielectric: this means that the confinement happens in a region much smaller than their propagation wavelength leading to a huge enhancement of non-linear optical processes like Raman effect.

There are two different kinds of plasmons, the propagating ones and the localized[25].
The first ones are extended along all the surface of a metal-dielectric interface and they decrease exponentially perpendicularly to the surface with a decay length of $1/\epsilon$.
Sensors based on this effect are often used for molecular recognition and disease immunoassays.
Differently Localized Surface Plasmons (LSPs) are excited on the surface of metallic nanostructures whose dimensions are much smaller than the excitation wavelength and their resonance is strongly affected by environment changes.

The particular characteristic of LSPs is that their wavelength is in the order of of microns, depending on the excitation, but as localized they cannot propagate more than the sizes of the metal structures (nm range) and so providing a very big enhancement of the field.

Surface plasmons are typically coming from nanostructures characterized by 1 or 0 dimensions like nanoparticles or nanorods[26].
When the incoming frequency matches the resonant wavelength of the plasmons (resonant

condition), a huge increase of absorption is gained; this effect can be easily observed looking at the absorption curve of the sample.

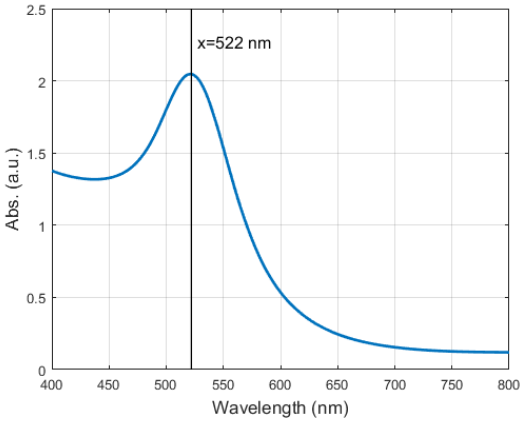

Figure 10: Typical absorption curve for a solution of plasmonic nanoparticles.

The best way to understand surface plasmons is to design the metal nanostructures (nanoparticle in the simplest case) like a forced mechanical oscillator[27].
The excitation in that case comes from the mechanical force and the response is given by the position of the center of mass.
In the parallel plasmonic system the excitation is the incoming electromagnetic wave (laser) and the response is the given by the polarizability of the nanoparticle.

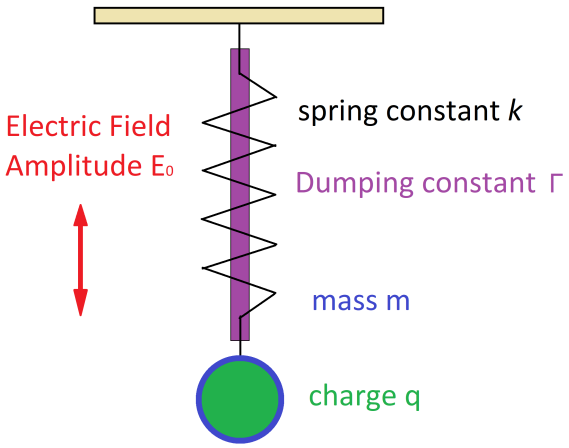

Figure 11: Driven damped oscillator representation.

Classical oscillator

The external force related to the excitation is in the form $f\cos(\omega t)$ and for the classical oscillator system, the equation of motion is defined as:

$$\ddot{z} + \Gamma\dot{z} + {\omega_0}^2 z = Fe^{i\omega t} \tag{24}$$

where $F = \frac{f}{m}$ *and* $\omega_0 = \sqrt{\frac{k}{m}}$ *the equilibrium frequency with k the spring constant and m the mass.*

The typical solution is in the form:

$$z(t) = z_0 e^{-i\phi} e^{i\omega t} \tag{25}$$

with ϕ the phase shift between response and excitation.

Solving the equation of motion it's possible to get the resonance of the response as:

$$\omega_{max} = \omega_0 \Big[1 - \frac{1}{8\pi^2}\Big(\frac{T_0}{\tau}\Big)^2\Big]^2 \tag{26}$$

Here T_0 is the self period of the free spring and τ is the inverse of the damping constant Γ.

It has to be noticed that the absorption of the spectra is not really a sharp peak and the resonance can be defined with a width of $\Delta\omega = \Gamma$ [27].

Retaking the excitation $f\cos(\omega t)$, the instantaneous quantity will be given by:

$$P(t) = \frac{\delta W}{\delta t} \tag{27}$$

And the average value is defined as:

$$< P >= \frac{1}{2} f z_0 \omega \sin\phi \tag{28}$$

The adsorbed power is maximum at the resonance and it can be shown that it corresponds to:

$$< P(\omega) >= \frac{\Gamma}{2m} \frac{\omega^2}{(\omega^2 - \omega_0^2)^2 + \Gamma^2\omega^2} f^2 \tag{29}$$

Then, considering a Lorentzian profile, the following simplifications can be done:

- $(\omega^2 - \omega_0^2)^2 \approx [2\omega_0(\omega - \omega_0)]^2$
- $\Gamma^2\omega^2 \approx \Gamma^2\omega_0^2$

Reaching the final formula of the mean absorbed power:

$$< P(\omega) >= \frac{\Gamma}{2m} \frac{\omega^2}{4\omega_0^2(\omega - \omega_0)^2 + (\Gamma/2)^2} f^2 \tag{30}$$

Nanoparticles

In the case of a nanoparticle the calculations can be exactly the same with the following analogies[27]:

	Oscillator	**Nanoparticle**
Excitation	Mechanical force $f\cos(\omega t)$	Electric field (wave) $E_1\cos(\omega t)$
Response	Center of mass position $z_0\cos(\omega t - \phi)$	Polarisation $P_1\cos(\omega t - \phi)$

Table 2: Analogies between oscillator and nanoparticle.

After this analysis and recording the formula from the average power in Eq. 28, it's possible to deduce the mean power absorbed by unit volume related to the nanoparticle as:

$$< P_{vol} >= \frac{1}{2} E_1 P_1 \omega \sin\phi \tag{31}$$

and noticing that the polarization is related to the electric field by $P = \epsilon(\omega) \cdot E$, we can finally reach:

$$< P_{vol} >= \frac{1}{2} \omega \epsilon_0 \epsilon_m(\omega) {E_1}^2 \tag{32}$$

Now let's analyze the confinement of a metal nanoparticle in a dielectric material under the effect of an external electric field.
Due to the dipolar behavior of the charges in the nanoparticles there will be a depolarizing field inside.

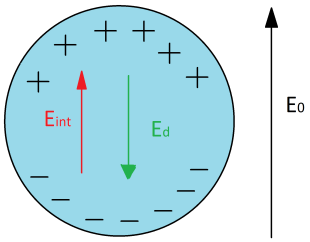

Figure 12: Electric fields acting on a metal nanoparticle.

The internal field can be seen as the sum between the external field and the depolarizing one:

$$E_{in} = E_0 + E_d \tag{33}$$

where E_0 is the external electric field and E_d the depolarizing field

Starting from applying the boundary conditions at the interface between gold and dielectric:

1. Potential continuous at the interface;
2. Normal component of **D** (Electric displacement field) continuous at the interface.

It's possible to compute the internal electric field as:

$$E_{in} = \frac{3\varepsilon_m}{\varepsilon + 2\varepsilon_m} E_0 \tag{34}$$

where ε_m the permittivity of the surrounding medium and ε the dielectric constant of the metal.

Combining Eq. 33 and Eq. 34 it will lead to:

$$E_d = -\frac{\varepsilon - \varepsilon_m}{\varepsilon + 2\varepsilon_m} E_0 \tag{35}$$

We can notice that:

- in the case of $\varepsilon > \varepsilon_m$ the depolarizing field opposes the external one;
- in the other case the two fields add constructively and the internal field is larger than the external one.

This effect represents a very important result, it means that for some wavelengths there is an amplification of the field in the nanoparticle.
This effect can happen only when a material is characterized by a negative dielectric constant like in the case of the metal.

Then we can combine the volume power absorbed by the sphere, derived with the mechanical oscillator analogy (Eq. 32).
The absorption cross section is defined as the ratio of the total power absorbed and the received flux:

$$\sigma_{abs} = \frac{< P_{vol} > V}{I_0} \tag{36}$$

$$with\ I_0 = \tfrac{1}{2} c \epsilon_0 \sqrt{\epsilon_m} {E_0}^2$$

Substituting the value of the internal field we can lead to:

$$\sigma_{abs} = \frac{9\omega V}{c} \frac{{\epsilon_m}^{3/2} \epsilon_2}{[\epsilon_1 + 2\epsilon_m]^2 + \epsilon_2^2} \tag{37}$$

If $\epsilon_2 \approx 0$ (verified in case of silver, an approximation for gold) the resonant condition happens for:

$$\epsilon_1 = -2\epsilon_m \tag{38}$$

Then using the Drude model for conduction electrons with $\Gamma << \omega$:

$$\epsilon_1(\omega_{SPR}) \approx 1 - \frac{\omega_p^2}{\omega_{SPR}^2} = -2\epsilon_m(\omega_{SPR}) \tag{39}$$

i.e.

$$\omega_{SPR} = \frac{\omega_p}{\sqrt{1 + 2\epsilon_m(\omega_{SPR})}} \tag{40}$$

Finally it's possible to define the local field factor f with:

$$f = \frac{E_{int}}{E_0} = \frac{local\ field}{applied\ field} \tag{41}$$

that in the case of an isolated spherical nanoparticles and in the quasi-static approximation is:

$$f = \frac{3\epsilon_m}{\epsilon + 2\epsilon_m} \tag{42}$$

This analysis explains that a nanoparticle can really act as a nanoantenna, opening many possible applications such as SERS, non linear optics, near-field microscopy, fluorescence enhancement, EM energy transfer...

In the last years plasmons become more and more powerful due to the parallel improvement of fabrication techniques for metallic nanostructures, leading to high quality and reproducible substrates that can exhibit huge enhancement.

As we saw a necessary condition to realize SPR is that the permittivitty of the the substance should be negative (as seen in metals) and the hosting medium (environment) must have a positive permitivitty.
The resonance is strongly dependent on the surrounding medium and can change with varying effective permittivity: this is actually why the surface plasmon resonance can be used directly as sensing technique.
The main idea is to detect a change in the dielectric constant on the surface with a shift in the resonant wavelength; this kind of technique will permit real-time analysis with high performance and high sensitivity at a very low fabrication costs.
The main drawback of this method is that is not qualitative, it can be used just in presence of a specific element to detect.
The main applications involves the gas sensing and to detect the adsorption of molecules on the surface (DNA, proteins...).

2.1.3 SERS

SERS (Surface Enhanced Raman Spectroscopy) consists in combining together the Raman effect and the surface plasmons resonance.
This technique was discovered in the 70s with the detection of pyridine on a rough silver surface[28].
In the following years a lot of studies on this subject has been carried out, in particular on the nanofabrication of metal nanostructures to reach very big enhancements of the field in order to overcome the low intensity of Raman effect.
SERS principle has not been completely understood yet, nowadays there are two main theories for its explanation:

A - Electromagnetic Theory

In this case the principle is based on the enhancement of the EM field at the metal-dielectric interface that happens when the incoming light matches the resonance wavelength of the Localized Surface Plasmon of the metal[26][29].
Hitting the surface, the light will excite different phenomena, in this case the enhancement will arise from two different effect:

- the incoming light will be enhanced among the surface, so the Raman signal will be increased;
- the Raman effect (and its signal) is then enhanced itself.

Considering these facts and giving an approximate enhancement factor of E^2 for each stage, the final result will lead to a E^4 final factor.
So when molecules are in proximity of the metal interface, they experience a big electric field that increases the Raman effect and provide an high output signal.
A simple formula can be written as following:

$$EF = \kappa(\lambda_{ex}) \cdot \kappa(\lambda_{sc}) \tag{43}$$

where EF is the total averaged Raman enhancement while λ_{ex} and λ_{sc} are the enhancements in the incident radiation and scattered one respectively.

The enhancement is maximized with the matching between the incoming radiation and the plasmon resonance at the surface. If not, the two effects cannot be coupled and the E^4 factor will not be reached.
Concerning this last sentence, the choice of the material becomes a fundamental issue in the device's optimization: usually gold and silver are exploited for SERS experiments due to their plasmon position between the visible and near-infrared range.

B - Chemical Theory

Here the signal enhancement comes from the increased polarizability of the molecules due to the charge transfer or the creation of a chemical bond between the analyte and the metal. This theory has been provided to explain some enhancement mechanisms that couldn't fit with the previous hypotesis, in particular concerning the fact the effect is molecule-dependent.

This theory is related with the charge transfer between the chemisorbed molecules and the metal[26][30].

For this purpose, the HOMO (Highest Occupied Molecular Level) and the LUMO (Lowest Unoccupied Molecular Level) of the molecule should be positioned symmetrically about the Fermi energy of the metal in order to make the transition possible.

SERS can be be divided in two main regions:

- Colloidal solutions of metal nanoparticles;
- Nanostructured metal surfaces.

The second way is becoming the most exploited due to its easiness to tune the resonant wavelength of the plasmon and to build specifically designed sensors.
This kind of surface can be obtained with the deposition of metal nanoobjects directly on a substrate or producing litographed pattern with arrays of nanostructures.

A general description of the enhancement factor is given by the formula[31]:

$$g^R = \left(\frac{\mid E(r) \mid^2}{\mid E_0 \mid^2} \right)^2 \tag{44}$$

where $E(r)$ is the local field and $\mid E_0 \mid^2$ the excitation electric optical-field amplitude.

Moreover the local factor can be written as:

$$I(r) = \frac{\mid E(r) \mid^2}{\mid E_0 \mid^2} \tag{45}$$

and $I(r)$ in the last formula accounts for the enhancement of the Raman radiation[32].

The efficiency of the Raman effect is strongly increased up to 10^8 times in the best cases[33], leading to the possible detection of a single molecule[34][35].

SERS spectroscopy is not only a matter of radiation, its enhancement is affected by a lot of parameters as for example the analyte composition, the excitation wavelength and the characteristics of the metal surface.
For this reason, every specific case should be further analyzed in details and supported by practical experiments.

2.2 Conical nanoporous membranes

The dynamics of particles characterized by Brownian motions has been widely studied in the last years due to the huge range of applications concerning the ionic transport at the micro and nano scale.
In the field of membranes and micro-channels entropic effects may plays a relevant role if highlighted in a proper way.

2.2.1 Principle of Brownian motion

The theory of Brownian motion can be used to describe the dynamics of non-equilibrium systems; the best way to reach this result is to use the Langevin equation, that consider the contribution of the friction and random forces.
The first concept of Brownian motion and, in particular, the relation between atomic and macroscopic properties were introduced by Einstein with the diffusion quantity[36]:

$$D = \frac{RT}{N_A 6\pi\eta a} = \frac{k_B T}{6\pi\eta a} \tag{46}$$

where R is the gas constant, N_A the Avogadro number, T the temperature, η the viscosity and a the radius of the particle. Finally the Boltzmann constant is defined as $k_B = \frac{R}{N_A}$

The main applications are ion channels, nano-porous materials, zeolites and microfluidic devices obtained with etching.

In the presence of channels or pores, the forces acting on the particles can be due to a gradient of concentration or an external applied force[37].
If we consider a force along the pores axis, it can be written as:

$$f = \mid f \mid e_x \tag{47}$$

where x stands for the axis along the channel.

Then the general equation of motion is defined as:

$$\frac{dr}{dt} = f + \xi(t) \tag{48}$$

with r the vector position of the particle, f the general force and ξ represents the random force.

The force $\xi(t)$ is used in order to describe the Brownian motion, taking in account a random force due to density fluctuations in the fluid; it is a stochastic variable and it accounts for the background noise in the fluids.
For this reason it is represented by the Gaussian white noise and it's characterized by the following mathematical properties[37]:

- $< \xi(t) >= 0$;
- $\langle \xi(t_1)\xi(t_2) \rangle = g\delta(t_1 - t_2)$

The typical system is developed along one axis, related to the particles motion and the idea is that, instead of a free diffusion in the host medium (liquid), the particles are subjected to a constrained motion, given by particular geometry of the system.

Here we will deal with bio-inspired membranes, whose principle consists in creating entropic barriers in the fluids that behave as a ratchet for molecules[38]; these particular properties permit to build nanodevices for smart ions transport or pumping for very promising applications[39][40].

In a confined medium, the transport is regulated by entropic barriers so the purpose is to create this ratchet starting from an asymmetry of the confinement.
In this kind of applications the membranes are subjected to a periodic voltage, with a zero value in average, and, exploiting this difference in the confinement, it's possible to have a rectification in the current, that means the flux is more favored along one direction[41].

The membrane is composed by a 10 µm polycarbonate layer characterized by pores with a conical shape and apertures of nm size. In order to reach this particularity the layer is first of all irradiated with heavy ions and then chemical etching at high temperature with caustic soda (NaOH) is performed in order to open the pores. This chemical attack is carried out only on one side of the membrane in order to create the conical shape.

2.2.2 Working Principle

The idea is to create entropic barriers acting in different ways for objects (ions, proteins...) of different sizes.
This role of entropy as a force for the transport can be exploited creating two kinds of asymmetries in the system:

- Conical nanopores;
- Ions with different sizes.

In the case of pores or channels, the molecules can be driven by a difference of concentration or by an external force (like an electric field for charged particles).
These two effects correspond respectively to a diffusion and a drift components that influence the flux of molecules, i.e. the current[39].
It can be written in the form:

$$J = -D\left(\nabla c + \frac{c}{k_B T}\cdot\nabla U\right) \tag{49}$$

where the first term is the diffusion one while the second is related to the drift. In particular D is the diffusion coefficient, c is the concentration and U is the potential energy.

As explained previously, entropy plays a relevant role in such a system and it's possible to evidence its contribution exploiting the free energy form:

$$F = U - TS \tag{50}$$

Keeping in mind that the force is defined as the gradient of energy, we can get the entropic force defined as $T\nabla S$.
Generally the entropy of a system is defined as

$$S = k \cdot ln(\Omega) \tag{51}$$

where Ω is the number of microscopic configurations (states) that can be adopted by the system.

In our case we have to consider the cross section area in the nanopores, in order to characterize the entropic force that is acting.
Considering a fixed x position, the accessible area will give the number of possible occupational states for the particles and the entropy can be written as[39]:

$$S = k \cdot ln(\Omega) = k \cdot ln\left(\frac{A(x)}{a}\right) \tag{52}$$

where $A(x)$ is the cross-section area accessible for the particles depending on the x position while a is the unit area.

To understand the concept of accessible area we should consider the depletion layer at the pores sides; the center of mass of an ion cannot approach to the border more than its radius. This happens when the size of the channel is comparable with the ion radius (tip of the conical pore) and it will lead to different accessible areas for ions with different size; as a consequence, also the entropic force will change directly in the same way.

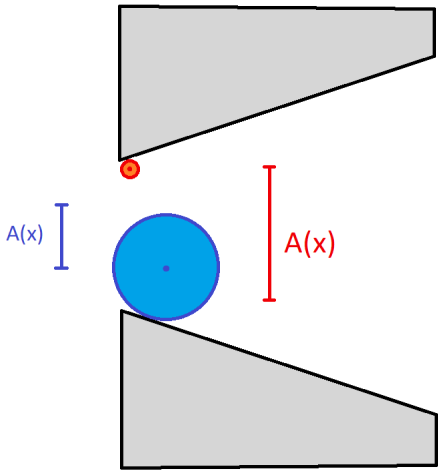

Figure 13: Different accessible areas A(x) for different ions size.

In general the accessible area for a circle (cross-section of a conical pore) is given by:

$$A(x) = \left(\frac{d(x) - 2r}{2}\right)^2 \pi \tag{53}$$

where d is the distance between the two borders (at a given position) and r is the radius of the ion.

So increasing the size of the particle, we decrease the accessible area $A(x)$ and, as a consequence, also the entropic force (See eq. 52).
This effect will lead to different entropic barriers for varying ions size, as it's possible to see from the figure 14.

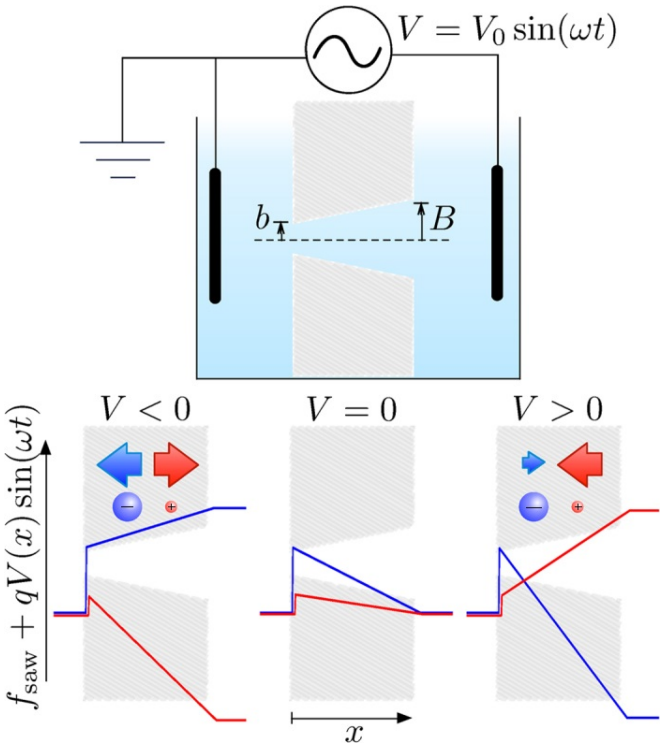

Figure 14: Working principle of conical nanopores for alternate voltage[39].

In particular here the case of large anions and small cations is analyzed. Looking at the negative charged molecules (blue) we can study their behavior in the three cases of applied voltage:

- V=0 : the particles feel the potential barrier in both direction due to the shape of the cone, so in principle there is no flux between the two compartments;
- V<0 : the potential barrier is now compensated by the electric field and the negative charged molecules can flow in the left compartment, towards the cone tip;
- V>0 : due to the conical shape there is still a potential barrier for the molecules to flow on the right side, leading to a small amount of current towards the big side of the cone.

So the ionic current in the case of positive and negative value is different, leading to a rectification the that can be seen from I-V plots of the alternate applied voltage.
A rectification means that one direction of the flux is more favorite than the other one, obtaining different values of current for the same amount of voltage but opposite in sign.
This concept can be applied in the same way for the cations, obviously with opposite direction. Anyway, considering smaller ions, the difference of accessible area will be smaller, leading to a reduced entropic barrier and so a smaller effect and rectification.
This is the second crucial point: for $V > 0$ the energy barrier of anions at the end of the cone (tip) is bigger than the one for cations in the case of $V < 0$.

We can so deduce that the entropic barrier is size-dependent and it acts differently for ions with different characteristics (mass, charge, diffusion..).

The rectification of a system is given by [39]:

$$\alpha = \frac{J_0^+ + J_0^-}{\mid J_0^+ \mid + \mid J_0^- \mid} \tag{54}$$

where $J_0^{\pm}$ is the current computed for a tha same voltage but with opposite sign.

In our case the pore walls are negatively charged, so the first step consists in using a macromolecule that carries negative charge in order to avoid any possible adsorption on the walls and having a repulsive behavior.

2.2.3 Rectification and Pumping

After having observed a rectification in the current, so the presence of a favorite direction for the ion flux, it's possible to start to think about the process as a pumping effect, leading to an enhancement of concentration in one side.

Let's consider the case of ions in solution with diffusion coefficient $D = kT\mu$, with kT the thermal energy, $\mu = 1/(6\pi\eta r_h)$ the mobility of ions (velocity per unit of force i.e. the reverse the friction), η the viscosity of the solution and r_h the hydrodynamic radius of ions.

When an electric field E is applied, the velocity v of ions comes from the balance between friction and electric force:

$$v = \mu q E \tag{55}$$

with q the the net-charges carried by one ion.

Considering an ion solution with initial concentration c, the current J_x of ions (so the number N of ions per unit of area and time) moving through a plane at position x experiencing a potential gradient $\nabla\mathcal{U}$ is the sum of brownian diffusion $-D\nabla c_x$ and drift motion $-c_x\mu\nabla\mathcal{U}$:

$$J_x = -D\nabla c_x - c_x\mu\nabla\mathcal{U} \tag{56}$$

with

$$\nabla\mathcal{U} = q\nabla U + \nabla\mathcal{E} \tag{57}$$

In particular the term $\nabla\mathcal{U}$ is composed the sum of the applied electric potential gradient $q\nabla U$ (product of electric field for the ion charge) and of additional energy gradient $\nabla\mathcal{E}$ that contains all the interaction energy terms between the membrane and the ions (electrostatic potential due to pore wall, entropy effect etc..). This last term can eventually be different for the two directions of motion due to the anisotropy of the system.

In our experiment we will have two compartments (denoted with subscripts 1 and 2) of volume v_i and concentration c_i, separated by a porous membrane of thickness h and surface of exchange of area A.
The total number of ions in the system is:

$$N_T = v_1c_1 + v_2c_2 \tag{58}$$

and the total concentration:

$$c = N_T/(v_1 + v_2) \tag{59}$$

Also, we consider an oscillatory voltage difference U across the membrane. The indexes $+$ and $-$ will be use to indicate quantities related to the sign of U.
After one period, the net current $\mathcal{J}$ through the membrane is

$$\mathcal{J} = \frac{J^+ + J^-}{2} \tag{60}$$

Also, as $\nabla U^- = -\nabla U^+$, from Eq.57 the average potential gradient over one period is

$$\nabla\mathcal{U} = \frac{\mathcal{U}^+ + \mathcal{U}^-}{2} = \nabla\mathcal{E} \tag{61}$$

So in this case we can write the equation 56 as

$$\mathcal{J} = -\frac{D}{h}(c_2 - c_1) - \mu\nabla\mathcal{E}\frac{(c_2 + c_1)}{2} \tag{62}$$

or

$$\mathcal{J} = -\left(\frac{D}{h} + \frac{\mu\nabla\mathcal{E}}{2}\right)c_2 + \left(\frac{D}{h} - \frac{\mu\nabla\mathcal{E}}{2}\right)c_1 \tag{63}$$

The two concentrations can be linked with the total number of ions $N_T = v_1c_1 + v_2c_2$, so we can write c_1 as a function of c_2:

$$c_1(t) = \frac{N_T}{v_1} - \frac{v_2}{v_1}c_2(t) \tag{64}$$

Combining Eq. 63 and Eq. 64, the net current becomes

$$\mathcal{J} = \left(\frac{D}{h} - \frac{\mu\nabla\mathcal{E}}{2}\right)\frac{N_T}{v_1} - \left[\frac{D}{h}\left(1 + \frac{v_2}{v_1}\right) + \frac{\mu\nabla\mathcal{E}}{2}\left(1 - \frac{v_2}{v_1}\right)\right]c_2(t) \tag{65}$$

If we consider the current as the ions flowing through the exchange area it assumes the form:

$$\mathcal{J} = \frac{1}{A}\frac{dN}{dt} = \frac{v_2}{A}\frac{dc_2}{dt} \tag{66}$$

Finally combining eq. 65 and eq. 66 we get the differential formula:

$$\frac{dc_2}{dt} = K_1 - K_2c_2(t)$$

$$\text{with} \begin{cases} K_1 = \dfrac{A}{v_1v_2}\left(\dfrac{D}{h} - \dfrac{\mu\nabla\mathcal{E}}{2}\right)N_T \\ \\ K_2 = \dfrac{A}{v_1v_2}\left(\dfrac{D}{h}(v_1 + v_2) + \dfrac{\mu\nabla\mathcal{E}}{2}(v_1 - v_2)\right) \end{cases} \tag{67}$$

whose solution is in the form:

$$c_2(t) = \frac{K_1}{K_2} - \left(\frac{K_1}{K_2} - c_2(0)\right)e^{-K_2t} \tag{68}$$

Considering the limit case for time $t \to \infty$, $c_2(t)$ reaches a plateau value K_1/K_2 which is equal to

$$c_2(\infty) = c\left(\frac{1 - \dfrac{h\nabla\mathcal{E}}{2kT}}{1 + \dfrac{h\nabla\mathcal{E}}{2kT}\gamma}\right) \text{ with } \gamma = \frac{v_1 - v_2}{v_1 + v_2} \tag{69}$$

The quantity in parenthesis is the concentration magnification factor (higher than 1 for $\nabla\mathcal{E} < 0$). The characteristic rate K_2 to reach equilibrium can be written as

$$K_2 = \frac{AD}{h}\frac{v_1 + v_2}{v_1v_2}\left(1 + \frac{h\nabla\mathcal{E}}{2kT}\gamma\right) \tag{70}$$

Let us consider the case of same concentration $c_1(0) = c_2(0) = c$ on both sides of the membrane at time $t = 0$. In this case the equation 62 becomes

$$\mathcal{J}_0 = -\mu c\nabla\mathcal{E} \tag{71}$$

At time $t = 0$ the device can be characterized by the rectification efficiency α_0 defined as:

$$\begin{aligned}
\alpha_0 &= \frac{J_0^+ + J_0^-}{\mid J_0^+ \mid + \mid J_0^- \mid} = \\
&= \frac{\mathcal{J}_0}{\frac{1}{2}\left(\mid J_0^+ \mid + \mid J_0^- \mid\right)} = \\
&= \frac{-\nabla\mathcal{E}}{\frac{1}{2}\left(\mid q\nabla U + \nabla\mathcal{E} \mid + \mid -q\nabla U + \nabla\mathcal{E} \mid\right)} \\
&= \frac{-\nabla\mathcal{E}}{\frac{1}{2}\left(\mid q\nabla U \mid + \mid \nabla\mathcal{E} \mid + \mid\mid q\nabla U \mid - \mid \nabla\mathcal{E} \mid\mid\right)}
\end{aligned} \tag{72}$$

Assuming that ions always follow the direction imposed the electrostatic force that means $\mid q\nabla U \mid > \mid \nabla\mathcal{E} \mid$, finally the equation 72 gives:

$$\alpha_0 = \frac{-\nabla\mathcal{E}}{\mid q\nabla U \mid} \tag{73}$$

which permit us to estimate $\nabla\mathcal{E}$ in Eq.69 and 70 from a simple measurement at time $t = 0$. This result is a direct relation between the rectification and the energy gradient along the membrane, keeping in mind that $q\nabla U$ is known.

2.2.4 Analysis in temperature

Looking at the last result obtained, we can see the direct relation between the rectification and the energy gradient between the membrane and the ions; this means that computing the rectification from an experimentally obtained I-V curve, it's possible to give an estimation of the energy interaction.

Anyway this analysis doesn't give an estimation of the entropic contribution because the energy gradient is due to every kind of interaction between membrane and ions.
So we can try to define a gradient of energy that accounts for all the interaction terms, that are mostly the supposed entropic contribution and the electrostatic energy.
It can be written as:

$$\nabla \mathcal{E} = A - T \cdot S \tag{74}$$

where A is the electrostatic interaction, T is the temperature and S the entropy

The electrostatic energy is inversely proportional to the dielectric constant of the surrounding medium (water in our case) and it is defined as:

$$A = \frac{B}{\epsilon(T)} \tag{75}$$

where B is a constant and ϵ varies with the temperature, it decreases[42].

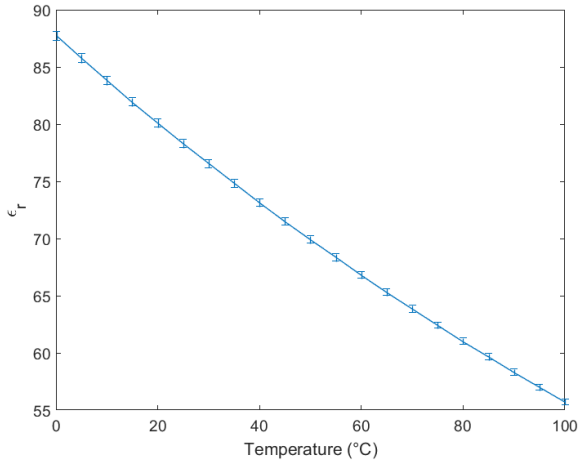

Figure 15: Dielectric constant as a function of temperature[42].

So we reach the form:

$$\nabla \mathcal{E} = \frac{B}{\epsilon(T)} - T \cdot S \tag{76}$$

Then considering the linear relation carried out in the previous chapter between the rectification and the energy gradient (Eq. 73), it's possible to combine it in the equation 76 obtaining:

$$\alpha \cdot \mid q\nabla U \mid = T \cdot S - \frac{B}{\epsilon(T)} \tag{77}$$

where $\mid q\nabla U \mid$ is constant for a given voltage.

From this simple estimation of the energy we can see that the entropic contribution $T \cdot S$ will be more important at higher T, while the electrostatic effect can be predicted considering the variation of the dielectric constant.
This kind of analysis can give us an estimation of the entropic term, more generally we are able to appreciate from which kind of interaction the rectification it's coming from.

2.3 Proteins

Proteins are large biomolecules composed by amino acids linked together by an amide bond (peptide). In particular every amino acid contains a carboxyl group (-COOH) and a free amino group (-NH_2) [43].
The amide bond consists in the linking between a carboxyl group and a amino group (CO-NH).

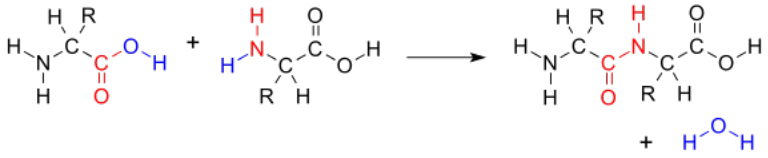

Figure 16: Peptide bond (in red) between two amino acids, from https://en.wikipedia.org/wiki/Peptide_bond.

There are 20 kinds of amino acids and the properties of their residues directly affect the function of the protein.
We can distinguish four levels of organization of a protein[43]:

- *Primary Structure*: the polypeptide chain, so the sequence of amino acids composing the protein. The composition and the order of the amino acids influence completely the 3-D structure and so the final functionality.
- *Secondary Structure*: repetition of local structures that can arrange in different ways like α-helix, β-sheet or random.
- *Tertiary Structure*: this is the folding and packing of secondary structures and directly controls the function of a protein. Its stabilization is reached with different types of interactions, in particular hydrogen bonds, disulfide bonds, ionic bonds and hydrophobic forces.
- *Quaternary Structure*: arrangement of tertiary structures into a single functional complex with non-covalent or S-S bonds.

Proteins have a large range of functions in the body, in particular as antibodies, enzymes, messengers, structural components and storage.
They are often used a biomarkers for monitoring any physiological activity in the human body and their role in diagnostics has become much more important in the last years.

An important physicochemical parameter that has to keep in mind when dealing with proteins is the isoelectric point, that represents the value of the pH at which a particular biomolecule is neutral, so it doesn't carry any electrical charge.
When the pH of the solution is smaller than the isoelectric point the protein is positively charged, on the contrary when it's bigger the carried charge is negative[26].

2.3.1 Raman spectra of proteins

Raman spectrum of proteins (and for biomolecules in general) typically ranges up to 3500 cm^{-1} shift from the excitation wavelength and from it it's possible to extract informations about the protein structure and interaction with the surrounding environment.
In particular the area between 400 and 1800 cm^{-1} represents the "fingerprint" region that permits to characterize and identify a specific protein, looking at the peak positions.
Then analyzing the intensity of a specific peak is possible to get the concentration of the investigated protein in the sample.

The most important Raman bands typical of proteins can be subdivided in 3 main groups that are amides, S-S stretching and aromatic amino acids[26].

Amides There are 9 modes related to the amide bonds, in particular A, B and I-VII amides. From this last kind the most relevant are Amide I,II and III.

- amide A band, related to NH stretching, around 3500 cm^{-1};
- amide B, also referring to NH stretching, about 3100 cm^{-1};
- Amide I : located between 1610-1700 cm^{-1}, it comes from the vibrations of carbonyl group (C=0) of the polypeptide chain and its position gives information about the secondary structure;
- Amide II : located between 1510 and 1580 cm^{-1}, it comes from the N-H bending and the C-N stretching and gives information about the conformation; in Raman technique this peak is quite poor.
- Amide III, located between 1200 and 1350 cm^{-1}, it comes from C-N bending and H-N stretching and it's correlated with the Amide I band.
- Amide IV, located between 625-770 cm^{-1}, coming from OCN bending;
- Amide V, 640-800 cm^{-1}, related to out-of-plane NH bending,
- Amide VI, 540-600 cm^{-1}, due to out-of-plane C=O;
- Amide VII, around 200 cm^{-1}, related to skeletal mode.

Anyway usually the first three amides are the most important and significant bands for a proteins, they permit to get the best informations related to the presence and the concentration of the biomolecule.

S-S stretching The bands related to the S-S bridges are in the range between 480 and 550 cm^{-1}.

Aromatic amino acids These vibrational bands are really sensitive to the environment variations, from their analysis it's possible to extract informations about the binding interaction.
There are a lot of different bands for vibrations related to different aromatic residues like Phenylalanine (Phe), Tyrosine (Tyr), Tryptophan (Trp) or Histidine (His) [26].

2.3.2 Bovine Serum Albumin

Albumin protein is the most abundant protein in blood and it's responsible for about 80% of the colloidal osmotic pressure[44].
BSA is a multifunctional transport protein, and so it's characterized by a broad affinity for many ligands; furthermore, albumin is used for transport and deposition of therapeutic drugs. This protein is widely used for studies due to its low cost and huge availability.

BSA is soluble in water and its primary structure contains a single polypeptide chain with 583 amino acid residues and a molar mass of 66.4 kDa. The secondary structure is characterized by roughly 67% R-helix structure and the rest is random[45].
Then the tertiary structure consists in nine loops stabilized by 17 internal disulfide bonds between 34 cysteine residues, resulting in three primary domains each containing one small and two large loops.
These disulfide bridges are the components for the compact N structure of BSA in the pH range from 4.5 to 8. This form of BSA is characterized by an axial ratio of 2.7, a molecular volume of about 88.25 nm^3 and a hydrodynamic radius of about 2.6 nm.

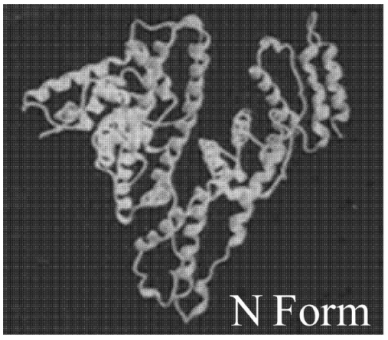

Figure 17: N-form structure of BSA[46].

At different ranges of pH the BSA is arranged into modified structures[47].
Under pH 4.5 a reversible unfolding happens leading to the F-form with a elongated shape, low solubility and high viscosity. Still decreasing the pH under 4 a new transition takes place arriving to the E-form that is completely extended.
Anyway at low pH more free thiol groups are accesible on the BSA surface, leading to increased coupling with nanoparticles.
Differently abobe pH 8 the protein reaches the B-form.

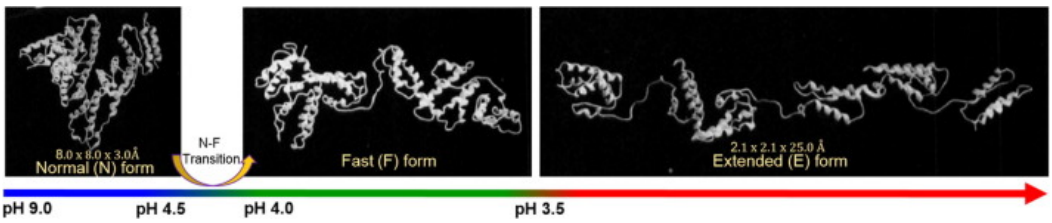

Figure 18: BSA conformation variations with pH [48].

The isoelectric point of BSA is at 4.7 and so it means that at the physiological pH (around 7) the

protein is negatively charged.

Here below is plotted the reference Raman spectrum of BSA with the related characteristic peaks.
The presented spectra are coming from the pure powder and from a solution of 1mM in buffer.

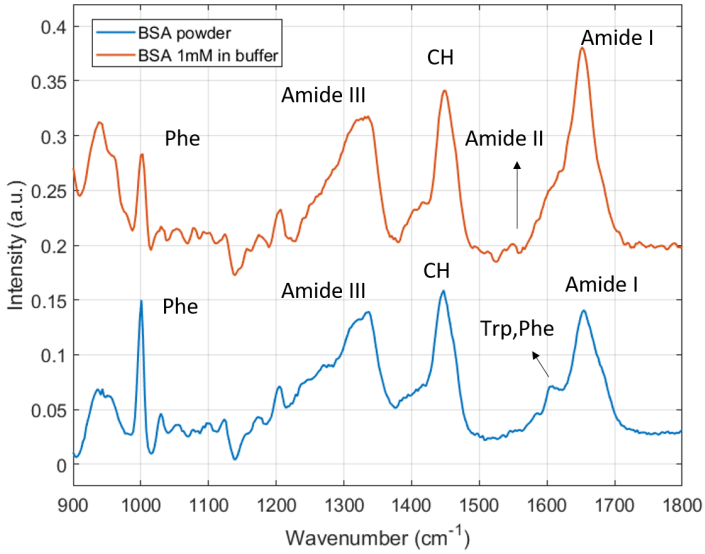

Figure 19: Raman spectrum of BSA taken in solution (1mM) and in powder [49].

The acquisition parameters related to figure 19 are:

- for the powder: 785 nm Laser, 100x objective (NA 0.90), 100% power, 100s;
- for the solution:785 nm Laser, 100x objective (NA 0.90), 100% power, 100s.

For the solution the Near-Infrared laser (785nm) is strictly needed in order to overcome the problem of fluorescence typical of proteins for lower excitation wavelength.

As it's possible from figure 19, the two spectra are basically the same but there are some variations due to different conformation and environment around the protein; in fact the blue spectrum is taken on the powder while the second one in solution.
The main difference is the appearance of the Amide II (even if very small) in the case of the solution while for the powder we can recognize a sharper peak concerning the vibration of Phenylalanine and Tryptophan residues at 1600 cm^{-1}.

2.3.3 Lysozyme

Lysozyme is an antimicrobial enzyme that plays a relevant role in the prevention of bacterial infections; in particular it attacks a specific component of bacterial cell walls, that is called peptidoglycan. This element is composed by a succession of amino sugars, N-acetylglucosamine (NAG) and N-acetylmuramic acid (NAM), that are crosslinked by peptide bridges. Lysozyme hydrolyzes these bonds increasing the bacteria's permeability and causing the bacteria burst[50].

Lysozyme is widely present in plants and animals[51]. The human one is found in the mucous membranes of the nasal cavity and tear ducts but also in saliva, tears, milk, cervical mucus,

leukocytes, and kidney tissue. Most of the lysozyme used for research purposes is obtained from hen egg whites.

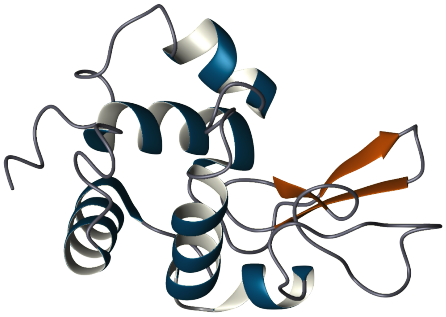

Figure 20: Representation of Lysozyme, from
http://www.bmrb.wisc.edu/featuredSys/Lysozyme/

The primary structure of lysozyme is composed by a single polypeptide that contains 129 amino acids; at the physiological pH the enzyme is organized in a compact and globular structure with a long cleft in the protein surface. This cleft is the active site that binds to the bacterial carbohydrate chain and then cleaves it[50].
The molecular weight of the lysozyme is 14.3 kDa and its isoelectric point is at 11.35 , making it positively charged at the physiological pH.

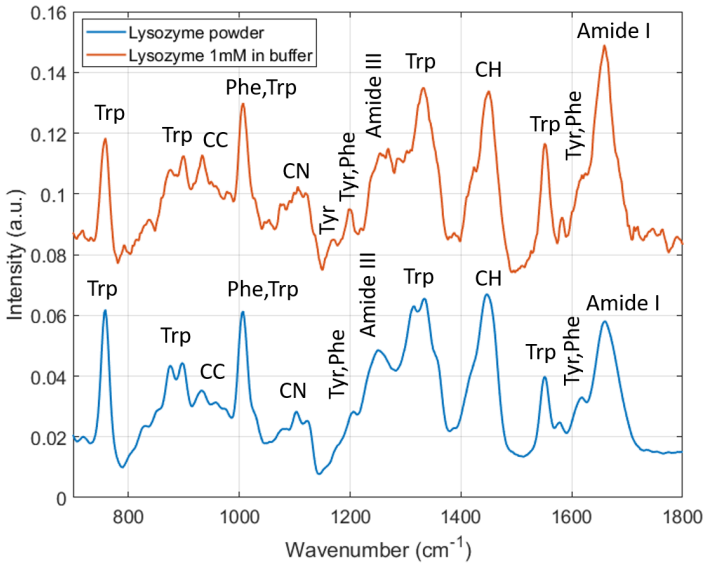

Figure 21: Raman spectrum of Lysozyme taken in solution (1mM) and in powder [49].

The acquisition parameters related to figure 21 are:

- for the powder: 785 nm Laser, 100x objective (NA 0.90), 100% power, 150s;
- for the solution: 785 nm Laser, 100x objective (NA 0.90), 100% power, 225s.

2.4 AFM basics

AFM (Atomic Force Microscopy) is a technique that provides a 3D image of a surface at the nanoscale, by measuring forces between a sharp probe (few nm) and surface at very short distance (0.1-10 nm).
With this technique is easy to reach the atomic resolution and it can be used for different purposes changing the configuration, for example to get different kinds of information, such as chemical, mechanical, electrical or magnetic[52].

In the classical configuration, the sharp tip obtained with microfabrication techniques is mounted on a cantiliver that follows a scanning path on the sample[53].
The deflection of the cantiliver is directly related to the force between the sample and the tip and it can be measured exploiting a laser and a photodiode; this will generate the topographic image of the surface.

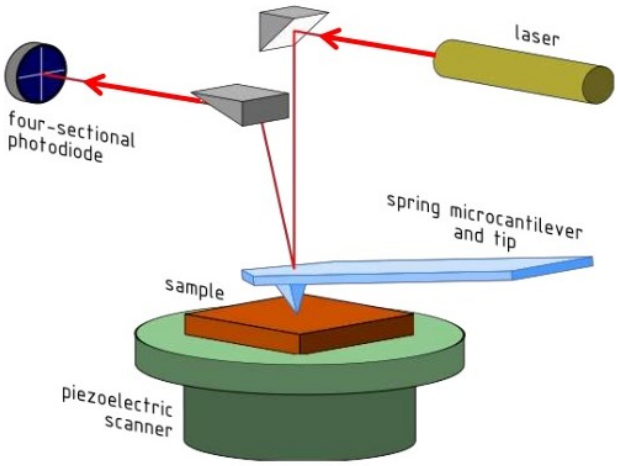

Figure 22: Basic working principle of AFM: the deflection of the cantiliver is measured by the laser on the photodiode, then it's possible to extract the 3D image of the surface. Taken from https://www.slideshare.net/joybiitk/atomic-force-microscope-fundamental-principles

The AFM can acquire the measurements in different ways, the most common are the contact mode or the tapping mode: in the first case the tip is in direct contact with the sample, in the second one the tip oscillates and the frequency will give the final information.
Generally AFM microscopy can be used for very different purposes, also spectroscopy in some case to analyse mechanical and chemical on a point of the surface; it can be used also to get informations about the material, such as stiffness, adhesion etc.

The main usages of this microscopy are related to:

- Inorganic materias, polymers and biological samples;
- Investigating the nanoscale changes of mechanical properties;
- Measuring the amount of force needed for removing an objects (nanoparticle) from a surface;
- Topographical informations.

In this case the acquisition used is the Quantitative Imaging mode, given by the JPK©apparatus.

2.4.1 QI Mode

The images for the proteins in liquid are acquired using the Quantitative Imaging (QI) mode given by JPK instrumentations; in this modality it's possible to reach the lowest peak forces down to 10 pN in order to preserve the sample and the tip from any damage[54].

QI mode records the complete curve force-distance for each pixel investigated and processing their variations it's possible to extract different informations about the sample.

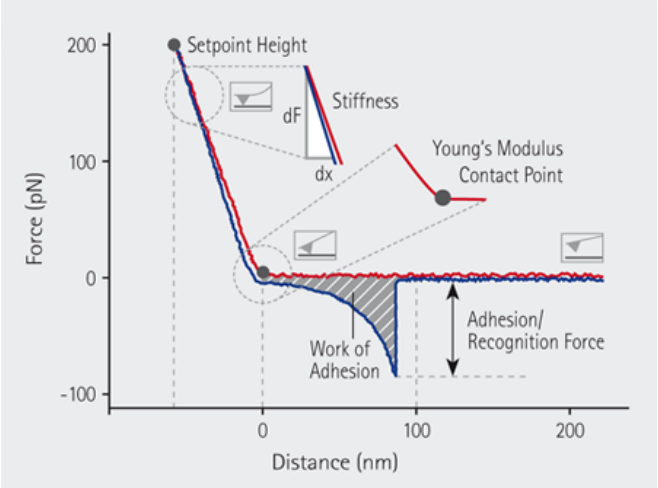

Figure 23: Working principle of the Quantitative Imaging mode: the informations about the sample come from the force-distance curves acquired in each pixel[54].

The red curve in the figure 23 represent the approach, while the blue is the retraction where the typical shape stands for the adhesion on the surface. For every investigated point, the indicated values can be extracted:

- the height;
- the stiffness, extracted by the slope;
- the adhesion;
- the Young's modulus of the material.

The advantage of this technique is the absence of lateral forces acting on the sample during the scanning, it provides good accuracy and very suitable for soft and sticky samples.

3 Methodology & Instrumentation

3.1 Instruments

3.1.1 Spectrometry

The available Raman spectrometer in the laboratory are:

- HORIBA© Xplora Raman spectrometer Olympus BX53;
- HORIBA© Labram Raman spectrometer Olympus BX40.

(a) HORIBA©Xplora spectrometer. (b) HORIBA©Labram spectrometer

Figure 24: Available spectrometers in the laboratory

.

The spectrometers are composed by three main components;

- Excitation source (laser);
- Sampling apparatus (optical microscope);
- Detector (CCD camera).

Regardind the excitation source, the possible wavelengths were 632 nm for the Labram and 660 nm or 785 nm regarding the Xplora.
For all the proteins in solution the Near-Infrared laser at 785nm is necessary in order to overcome the fluorescence; all the other samples are tested with all the wavelengths and then the one with the nicest spectrum is taken.
Concerning the plasmon measurements only the Xplora spectrometer has been used due to a better working.

The second point is the optical microscope, here the choice is between different lenses.
The most used were:

1. 80x magnification lens with a numerical aperture of 0.75 used for the Xplora spectrometer;
2. 100x magnification lens with a numerical aperture of 0.90 mounted on the Labram.

Raman measurements

When taking a Raman measurement, the laser impinges on the sample leading to the interaction between the molecules and the photons.
The spectrometer records the outcoming photons with the exploitation of a CCD camera and the software directly creates the acquired spectrum.

For this kind of measurement, the parameters subjected to variations are:

- **Laser power (%)**: it can be kept at 100% when dealing with a liquid solution while it should be decreased to 1% or 10% when dealing with SERS substrates in order not to burn or damage the sample.
- **Acquisition time**: it really depends on the investigated sample; sometimes (like for lysozyme) it should be kept quite high in order to be able to get a clear spectrum.
- **Number of acquired spectra**: this parameter just permits you to make more acquisitions in the same measurement and then the spectra are averages; this tool is very useful to decrease the noise in the spectrum but it affects of course the duration of the acquisition.

The proteins are always diluted in buffer, so deionized water with a mixture of salts, in particular weak acids and conjugate bases, that keeps the pH at a stable value; this will give more stability to the proteins too.
The used buffer is composed by Phosphate-buffered saline (PBS) solution at 10mM with the addition of 10mM of Magnesium Chloride ($MgCl_2$).

Plasmon resonance measurements

Concerning the plasmon measurement, the spectrometer works in transmission, collecting the light coming from the sample.
In order to get the plasmon resonance two measurements should be done:

- the first is done outside the sample, so on the glass substrate in this case;
- then a second acquisition with the equal parameters and without changing the working distance is carried out from the sample.

Finally the curve of the glass is divided for the sample one in order to evidence a difference in the absorption spectra.
This ratio creates the typical plasmon curve resonance.

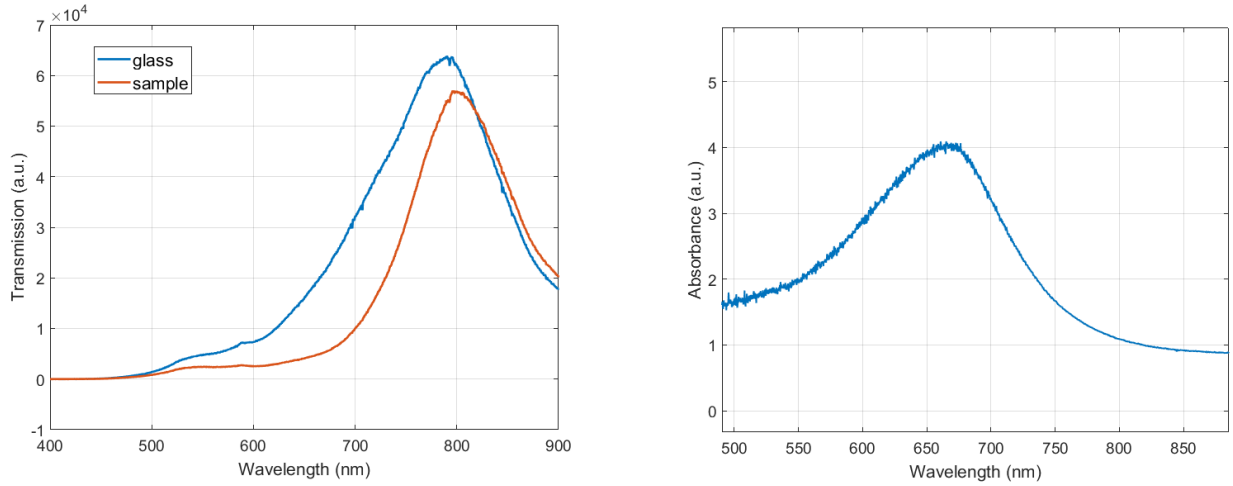

Figure 25: Procedure for the plasmon resonance analysis. First two transmission spectra are acquired on the glass and on the sample with the same conditions. Then, computing the ratio between the glass curve and the sample one, it's possible to get the absorption profile of the plasmons.

3.1.2 AFM

The exploited AFM microscope is the NanoWizard® 4 AFM from JPK ® instruments.

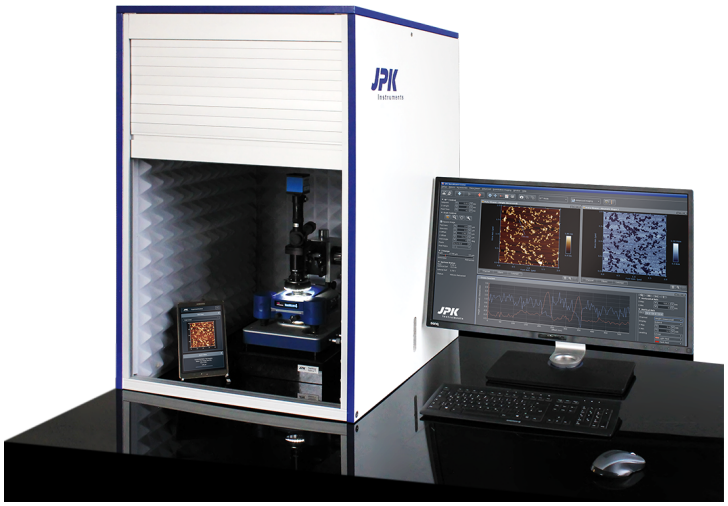

Figure 26: Configuration of the AFM JPK® apparatus.

This kind of configuration is very flexible and it represents a great possibility for imaging in liquid.
It gives many informations about the mechanical properties of the sample as adhesion, stiffness and elasticity. Moreover it can be arranged in different configuration for other kinds of experiments, for example Kelvin Probe AFM: this analysis permits to extract the workfunction of the sample and it's based on different surface effects.
A very useful characteristic is the integration of the optical apparatus that permits to get a fast result concerning the sample and it can be exploited for different purposes, even spectroscopic.

3.2 Membrane characteristics and preparation

The membrane is composed by a 10 µm polycarbonate layer that is first of all irradiated with heavy ions (Kr^{28+}); this bombardment is needed in order to weaken the structure of the film in certain point that will create the traces for the future pores.
The second step consists in performing a chemical etching at high temperature with caustic soda (NaOH) in order to open the pores.
To reach the conical shape of the holes the etching is carried out only on one side of the membrane, i.e. putting the Soda solution in one compartment and distilled water on the other one.
The working temperature is 60 °C and the soda solution is at a concentration of 2 M in water.
Two electrodes are used to make the OH^- ions attack the membrane; the electrical input is a DC voltage of 1 V and the ground is put inside in order to drive the negative ions.

The final configuration adapted consists in a plastic tube with the membrane pasted at the end (see fig. 27). The tube is then immersed in the Soda while the water is inside, making the cone tips of the pores addressed inwards.

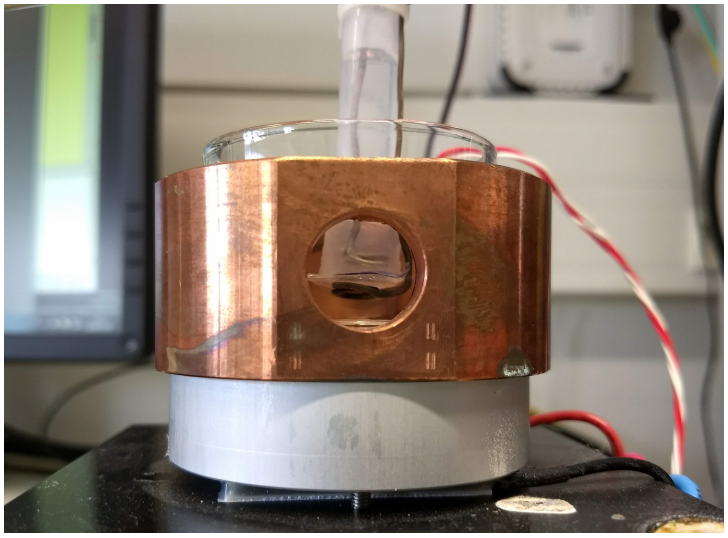

Figure 27: Set-Up for the chemical attack of the membrane. The big beaker contains the soda solution and the system around provides the right temperature; inside the small transparent plastic tube there is the distilled water.

To control the opening of the pores it's possible to look at the current between the two electrodes passing through the membrane.
At the beginning the pores are closed and so there is no current; when the etching process begins to work the pores start to open and the current is rising.
The end of the process is represented by a plateau value of the current, that means that all the pores are correctly open.
So it's possible to monitor the state of the membrane looking at the current, as shown in the figure 28.

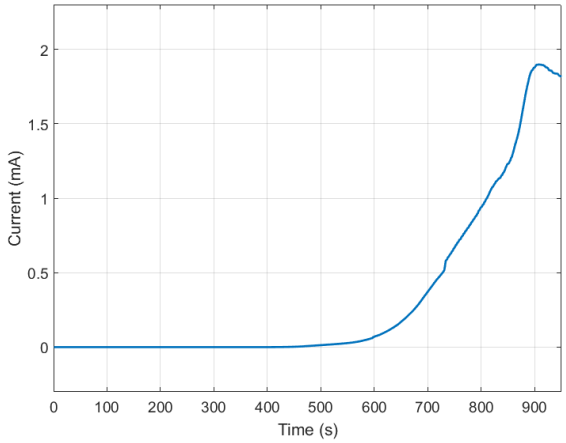

Figure 28: Current vs Time plot. When the pores are still close the current is zero, then it increases reaching finally a plateau value.

The size of the pores depends on the etching time and how much it's kept after the plateau value. Anyway the best way is to stop it just after reaching the plateau in order not to lose the conical shape of the pores.
The etching time is typically 15-20 minutes and the final current is in the order of few mA.

At the end the typical size of a pore has a radius of 200 nm on the bigger side and the other radius around 2 nm. The fluence of the used film is 10^7 pores/cm^2.

3.3 Gold Nanoparticles sample preparation

3.3.1 Colloidal solution

First of all a solution of Sodium Citrate ($Na_3C_6H_5O_7$) at 1% in distilled water is prepared.
Then a solution at 300 µM of $HAuCl_4$ in distilled water is prepared and made boiling with an heater plate. When it starts to boil, 0.4 mL of sodium citrate are added and the color will begin to become reddish.
Finally the color stabilizes after 5-10 minutes reaching the final configuration.

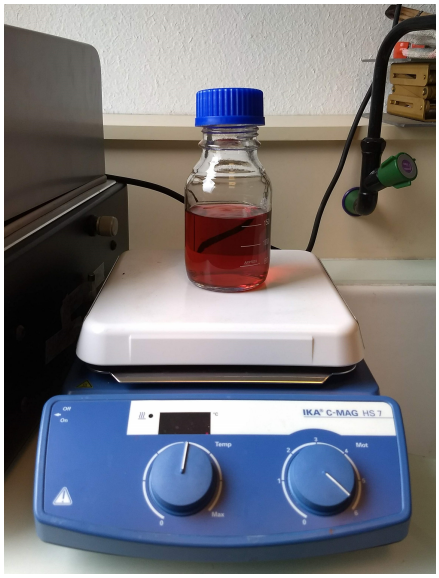

Figure 29: Solution of gold nanoparticles.

3.3.2 Sample preparation

After having cleaned the glass slides with acetone and ethanol, they are exposed to a UV-ozone cleaning in order to activate OH groups on its surface.
The second step consists in incubating the glass substrates in a solution 5% of MPTMS ((3-Mercaptopropyl)trimethoxysilane) in ethanol, in order to create a Self-Assembled Monolayer that acts as an adhesive for gold films and creates a uniform attachment of the gold nanoparticles.

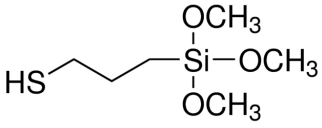

Figure 30: MPTMS chemical composition.

The solution is let incubating overnight on the glass, leading to the creation of a thiol monolayer.
The final step is the deposition of the colloidal solution of gold nanoparticles; in our case it has

a plasmon resonance at 532 nm, verified with a UV-visible spectrometer. The solution should incubate overnight and then rinsed with water.

3.4 Surface Functionalization with Aptamer

Proteins are alive in a wet environment, so for the incubation on the samples and analysis with the spectrometer they should be kept in the liquid.

The classical used incubation process takes usually 1 hour in order to be sure that the proteins are completely attached on the gold; it consists in directly put the sample inside the solution or putting a drop of 30 µL on the top and keep it in a humid chamber in order to avoid any possible evaporation.
Then the sample is rinsed with the same solvent used for the solution, PBS buffer in our case.

As it's possible to read in reference[55], BSA can be caught just incubating it directly on the gold sample due to the -SH group that are available on its surface. This permits to link the protein without causing its unfolding and so keeping its detectability with the Raman signal.

Differently from BSA, in the case of lysozyme there are less accessible -SH on the surface and it's more difficult to detect it with the previous described kind of incubation. In this case the linking with the pure gold is too strong and not controlled, leading to a complete unfolding of the protein.
For this reason a surface functionalization of the surface is needed.

A functionalization means modifying the surface with a biospecific element; to do this precise chemical procedures should be followed in order to reach the desired surface properties.
In our case a functionalization with aptamer is needed.

Aptamers are single-stranded DNA or RNA molecule that can bind targets with very high selectivity and specificity; they can assume a big different variety of shapes due to their tendency to organize in helices and loops. Aptamer functionalization is often used in the biosensing field due to this great fitting only with the specific target, allowing to detect a specific element in a heterogeneous sample. It can be used for proteins, carbohydrates, peptides and other biomolecules leading to sensors characterized by high selectivity.

Furthermore the aptamer molecules provide the right orientation of the attached proteins ensuring a consistent spectrum. Without them a random distribution of the absorption geometries would be inevitable leading to different spectra when changing the acquisition area.

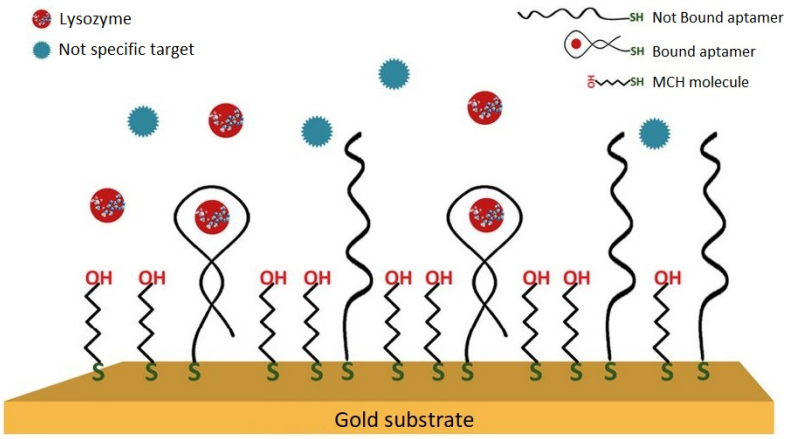

Figure 31: Self-Assembled-Monolayer created with the aptamer process. Please notice that the objects scale is wrong in this image, the elements are rescaled for an easier schematisation.

Here below are listed the steps used in the functionalization process:

1. Cleaning of the sample with the UV-ozone machine for 30 minutes;
2. Putting a drop of 30 µL of aptamer (with the final concentration of 2.72 µM) incubating for 1 hour on the sample. This step is repeated three times in order to be sure of the right attachment of the aptamer and the total coverage of the surface;
3. Putting a drop of 30 µL of MCH (6-mercapto-1-hexanol at 15 µM) incubating for 1 hour. This is a blocking molecule that is needed to fill the places not occupied by the aptamer in order to give it a precise configuration and so avoiding any random positioning.

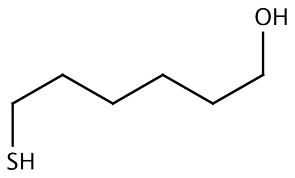

Figure 32: Representation of the MCH molecule.

4. Final incubation of the protein for 1 hour.

In the figure 31 is shown the final structure of the functionalized surface. In our case the aptamer is a specific one created for the lysozyme.

4 Results & Discussion

4.1 Filtration with the membrane

The first part of the work related to the membrane consists in the device optimization and then it will be tested with polymers.
The optimization is got trying different kinds of structures for the two compartments (plastic boxes, glass phials, eppendorf) and how to stick the membrane on the device (different kinds of glue, elastic garnish, teflon).
The idea is to reach the highest possible area of exchange (so of the membrane) and try to increase the volume difference between the two sides, always keeping the device in a convenient configuration for the experiments.
Finally the best setup found consists in pasting the membrane with a waterproof glue on one side of a polyethylene cylinder (1 cm of diameter) that contains 2-3 mL of liquid. The big volume depends on the used becher and it can be varied at preference.

Figure 33: Final device for the experiments: the membrane is glued at the end of the tube while the electrodes are fixed with plastic cable tie.

4.1.1 Polystyrene Sulfonate

The membrane is tested with Polystyrene Sulfonate (PSS) with a molecular weight of 200 kDa[1] at the physiological pH, so exploiting deionized water.
This polymer is soluble in water, its linear formula is $(C_8H_7NaO_3S)_n$ and the structure is shown in the figure 34 below.

[1]Dalton (Da) is a measure often used in biology. It corresponds to g/mol and it's used for the molecular weight.

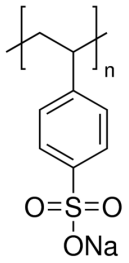

Figure 34: Structure of PSS.

The molecular weight of a monomer of PSS is 206 Da, meaning that in our case the polymeric chain is composed by roughly 971 monomers.

PSS in negatively charged in aqueous media, making it repulsive with respect to the pores walls (negatively charged).
A solution of 0.1 M in distilled water is prepared in parallel to a KCl solution at the same concentration. Theoretically the salt should not give any rectification due to the small size of the ions or at least not due to the entropic effect.
I-V curves are taken for the two solutions at room temperature (20 °C).

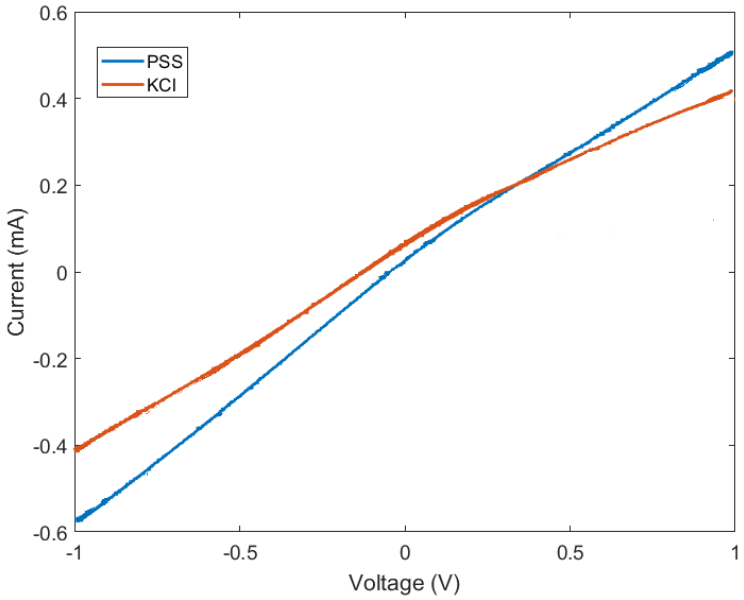

Figure 35: I-V curves at 20°C of two solutions of PSS (blue) and KCl (red) at 0.1 M, taken with a sinusoidal voltage between -1V and 1V.

Looking at figure 35, it's possible to notice a rectification for the PSS curve looking at the two extremities values of the current that are different for the same amount of voltage in modulus. For the KCl the rectification seems to be small looking at the current values but there is still a bending of the curve.

Anyway some considerations should be done:

- The membrane has been used for more trials and some KCl curves has been acquired after the PSS experiment, so the hypothesis of some PSS inside the pores cannot be completely excluded;
- in this kind of home-made system there are a lot of effects that are involved that can come from the electrodes not completely symmetrical, from capacitive effects and oxidation of electrodes so every measurement should be properly analyzed carefully;
- finally entropy in not the only factor affecting the symmetry of the flowing directions, a lor of other forces can modify the ions motion.

Focusing the attention on this last consideration it's possible to try to characterize the effects that are playing a role in such a system.
One fact that cannot be neglected is that the pores walls of the membrane are negatively charged at PH=7, so the behavior for negative and positive ions will be surely different due to electrostatic effects.
As demonstrated in the theory (Eq. 74), the gradient of energy that takes in account all the interactions can be written as:

$$\nabla \mathcal{E} = A - T \cdot S \tag{78}$$

whit A the electrostatic interaction, T the temperature and S the entropy

Then, as showed in the theory, we got the final relation (Eq. 77):

$$\alpha \cdot \mid q\nabla U \mid = T \cdot S - \frac{B}{\epsilon(T)} \tag{79}$$

where $\mid q\nabla U \mid$ is constant for a given voltage.

Analyzing the parameters in the previous formula:

- α can be computed by the I-V curves;
- $\mid q\nabla U \mid$ is constant for a taken voltage;
- T is known;
- S is the wanted quantity;
- B is a constant;
- ϵ is known;

So increasing the temperature and taking in account the variation of the dielectric constant with it, we can evidence the entropic contribution.
Exploiting the heating system, different I-V curves at increasing temperature are registered leading to the here plotted curves.

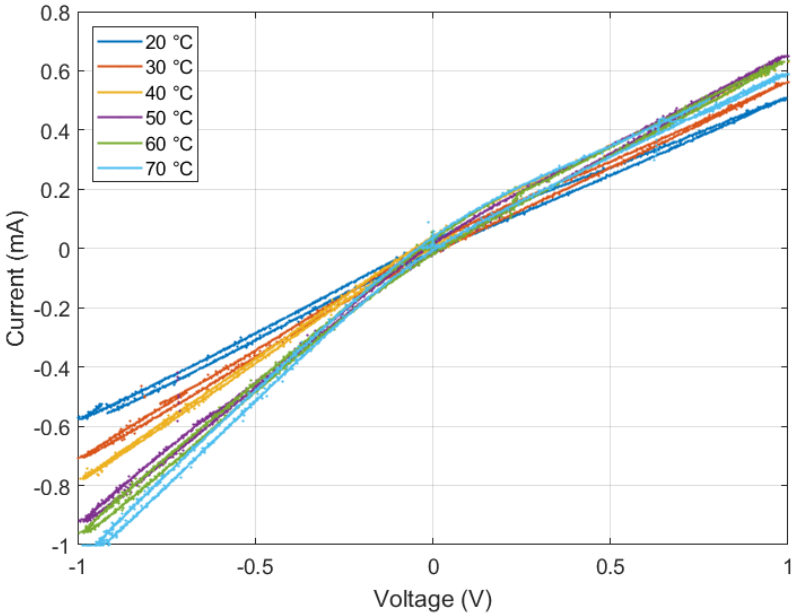

Figure 36: I-V curves for PSS 200k between -1 V and 1 V starting from 20 °C up to 70 °C.

As it's possible to see the value of the current is growing due to the increasing of the ions diffusivity with temperature.
From the curves it's not easy to understand if the rectification is increased or not, it should be extracted exploiting the usual method:

$$\alpha = \frac{J_0^+ + J_0^-}{\mid J_0^+ \mid + \mid J_0^- \mid} \tag{80}$$

where J_0^+ and J_0^- are the currents registered at one value of the voltage opposite in sign but equal in modulus[39].

Before extracting the value the curves are fitted and with this formula we have a value of rectification for every voltage registered.
We select the rectification related to 0.9 V because at higher value sometimes the current it's saturated.
All this process is carried out also for the KCl solution at the same concentration and then they are plotted together normalizing with respect to the dielectric constant of water.
The rectification is plotted versus the temperature, so looking at the equation 79 we can see that the slope of the curve will give the entropic contribution.

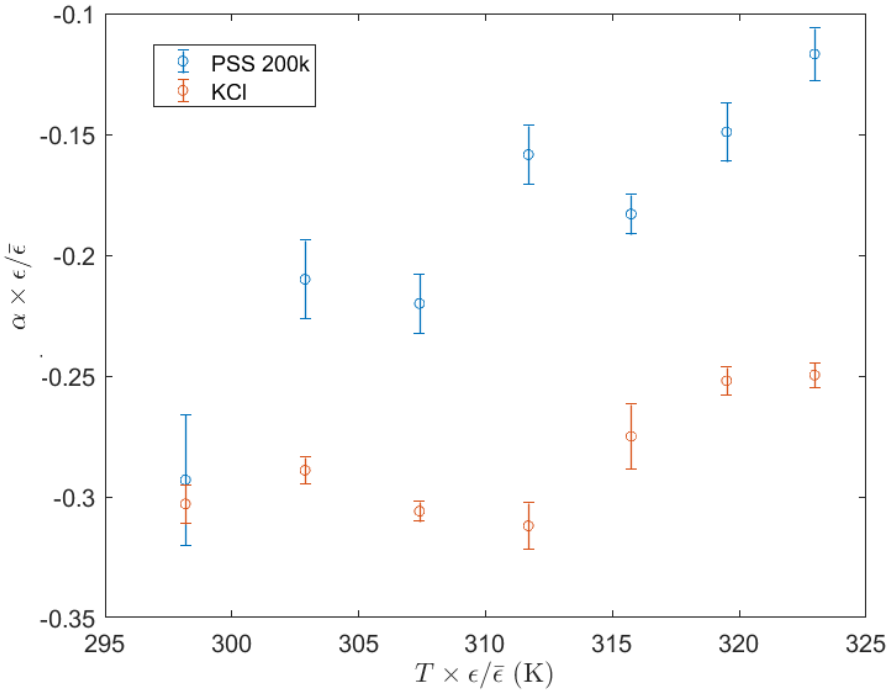

Figure 37: I-V curves for PSS 200k between -1 V and 1 V starting from 20 °C up to 70 °C.

The final result in figure 37 evidences how the entropic effect is affecting the rectification of PSS as a function of temperature: in this kind of plot the slope represents the entropic term. Looking at the KCl case the rectification is almost constant and the slope is really small, showing that we cannot suggest any possible entropic contribution due to the conical shape of the pores. Differently for PSS the slope is much bigger and there is a relevant variation between the starting and the final values.
This analysis suggests of an entropic term that helps the polymers going in one direction and affects their return; in particular this term is much more relevant for the case of PSS due to the bigger size of the ions involved.
This result permits to smartly evidence the entropic forces acting in isolated systems; these effects are caused by a smaller probability to approach the cone tips due to reduced accessible area.

4.2 Detection with AFM

One possibility to get an idea about the surface coverage of gold by the proteins consists in using AFM spectroscopy in liquid to visualize the proteins.
This technique could be used to characterize the effective attachment of the protein on the gold substrate. What is fundamental is to carry out the acquisition in a liquid environment (buffer) in order to keep the proteins in there native configurations.

QI mode is very suitable for imaging in liquid and soft materials such proteins that are quite fragile.
The investigation is first done on a bare gold surface and then protein at very low concentrations are added.
Here are presented the results coming from the BSA on gold.

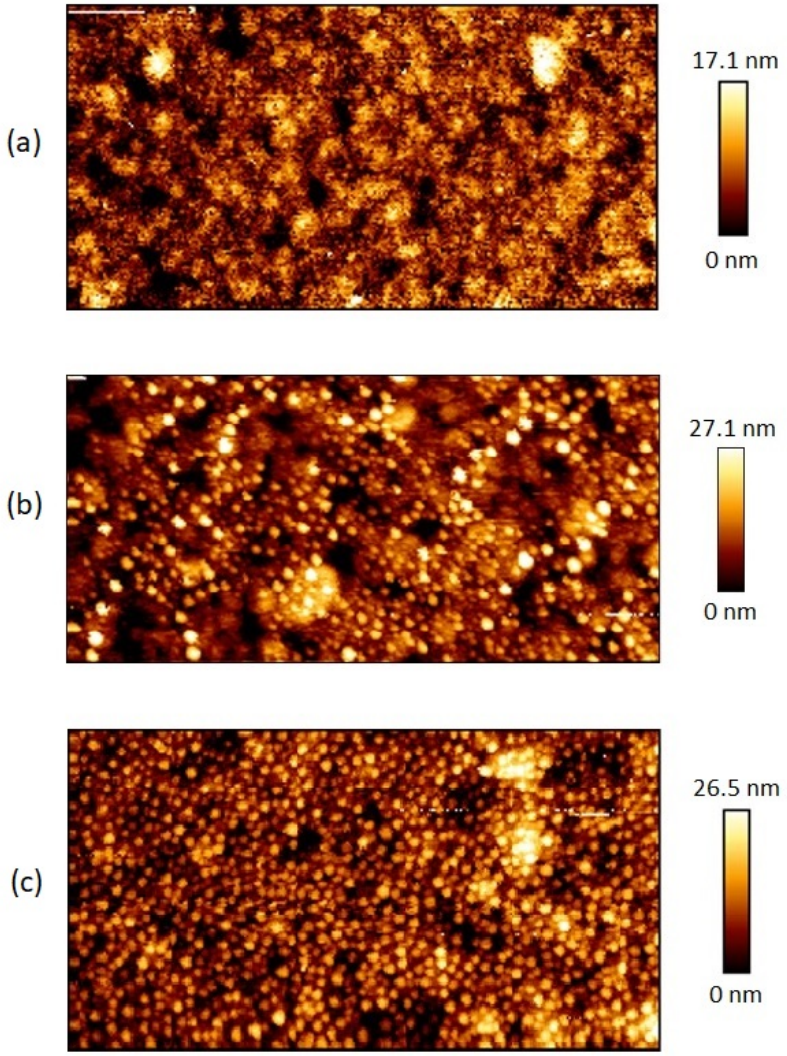

Figure 38: 2µm x 1µm AFM images of gold substrate for: (a) bare substrate (b) 20 nM of BSA (c) 200 nM of BSA.

Looking at figure 38, we can see that the gold substrate is quite rough, anyway no particles on it.
After the incubation in 20 nM of BSA we can already appreciate some isolated agglomerations of proteins with a characteristic size of roughly 30 nm.
Then increasing the concentration of a factor 10 we can notice almost a monolayer composed by nanoparticles of BSA on all the gold surface.

With this kind of analysis it's possible to understand that the gold surface will be completely covered by the proteins after 200 nM.
Using the AFM at very low concentration could be really a kind of technique useful to characterize the amount of proteins in the sample; exploiting the software ImageJ it's possible to estimate the percentage of protein on the total area for very low concentrations.
Anyway after 100 nM it becomes hard to guess the right amount due to the creation of a uniform layer of BSA. Moreover this analysis can be performed only when dealing with samples composed by just one particular element, it's not a qualitative technique.

What we can still deduce from this result is that in general BSA "sticks" on gold quite well due to the SH groups in the cystein residue available on its surface.
A further step is to verify that the protein is not completely denatured but still in a detectable configuration for the Raman detection.

4.3 Characterization of SERS substrate

The goal of the biosensing side of the work was to find a substrate able to detect a specific protein.
For this purpose we have different samples with very different enhancement ways and conformations to characterize giving an approximated value of the enhancement factor; this value represents the gain that is possible to achieve in terms of intensity when exploiting a SERS substrate instead of a Raman measurement (solution or powder).
In order to get this parameter all the samples were first investigated with a Raman reporter, the MBA molecule (4-Mercaptobenzoic acid), whose structure is shown in the figure 39 below.

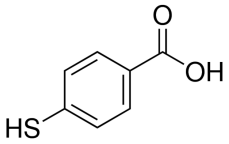

Figure 39: MBA molecule chemical structure $HSC_6H_4CO_2H$.

This molecule is often for the samples characterizations due to simple reasons:

- It can easily bind to gold to the -SH groups available in its structure;
- It has a very high Raman cross-section leading to a very easy detection;
- It shows a clear spectrum with two main peaks around 1080cm^{-1} and 1600cm^{-1}.

The enhancement factor of the samples is computed with respect to the Raman reference spectrum of MBA in powder, acquired without any SERS substrate.

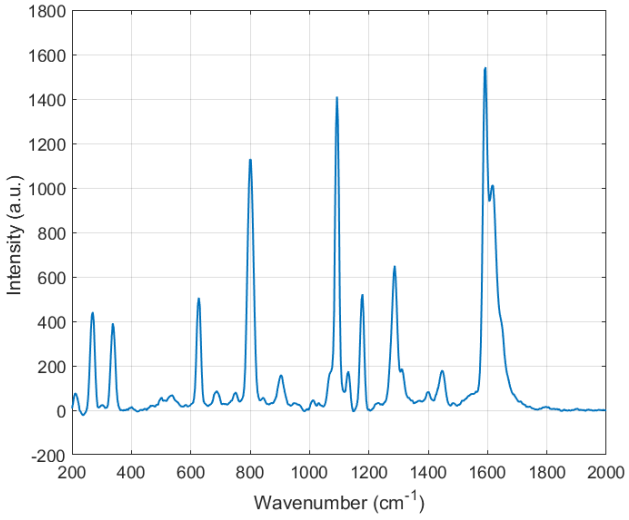

Figure 40: MBA Raman spectrum taken in powder with the 660nm laser, power at 1% and 40 s of acquisition

The two compared spectra (SERS and Raman) are taken really in the same condition, with the same laser and same lens in order to delete any possible differences in the acquisition.

The formula used for the computation of the parameter is[55]:

$$G = \left(\frac{N_2}{N_1}\right)\left(\frac{I_{SERS}}{I_{ref}}\right) \tag{81}$$

where N_2 is the number of molecules excited within the volume of the laser waist on the crystal of MBA powder and N_1 is the number of molecules contained in the monolayer deposited on the substrate illuminated by the laser spot. Then, I_{SERS} is the intensity of the analyzed Raman peak of MBA on the substrate and I_{ref} is the intensity of the same band in the MBA solution.

The intensities of the peaks are computed integrating the area under the peak at 1600cm^{-1}. Concerning the number of molecule deposited on the sample we can guess the presence of a monolayer that fully covers the top of the gold areas of the sample; for this reason we need to compute the percentage of gold on the total area on a specific sample. This is done exploiting the software ImageJ on the AFM images.

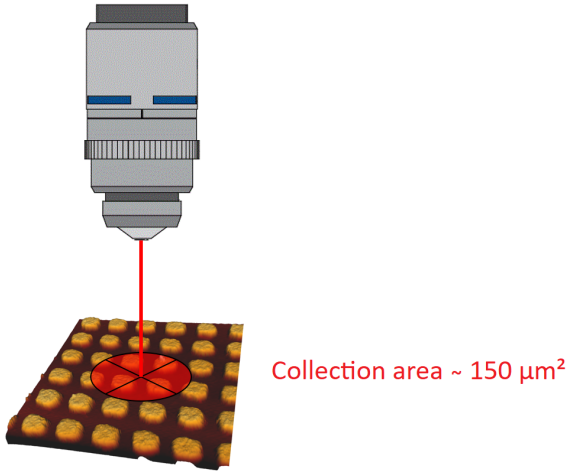

Figure 41: Scheme of the laser on the sample. Please notice that dimensions don't represent the real scale.

The collection area of the laser is computed getting the final value around 150 µm ^{2} (Fig. 41). For the SERS substrate the concentration of the MBA solution is 1mM, at this concentration all the gold should be covered by an uniform layer of molecules.
Concerning the powder, the number of molecules is obtained considering a depth penetration of the laser of 12 µm [55] and the collection area of 150 µm ^{2}.

In all this section the plots are rescaled and shifted up for a better visualization. This adjustment is done taking in account the time exposure, the laser power, the magnification and the numerical aperture of the objective.

4.3.1 Nanoimprinted Gold nanocylinders

The first tried sample comes from the LTM (laboratoire des technologies de la Microélectroniques) in Grenoble and it's composed by arrays of gold nanocylinders (see figure 42) deposited with a nanoimprinting technique.
This lithography technique is a method for fabrication of nm size patterns; it is a simple process characterized by low cost, high throughput and high resolution.
The working principle is the mechanical deformation of imprint resist and following processes.
The typical diameter of the nanocylinders is around 200 nm, their height roughly 70 nm and they are separated by a gap of 50 nm. Their plasmon resonance is at 673 nm.

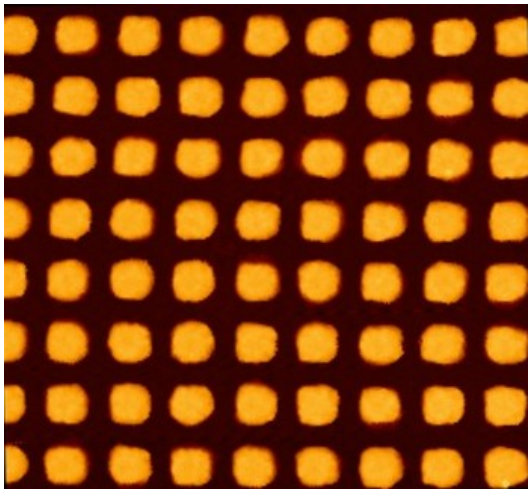

Figure 42: 3µm x 3µm AFM image of the nanocylinders.

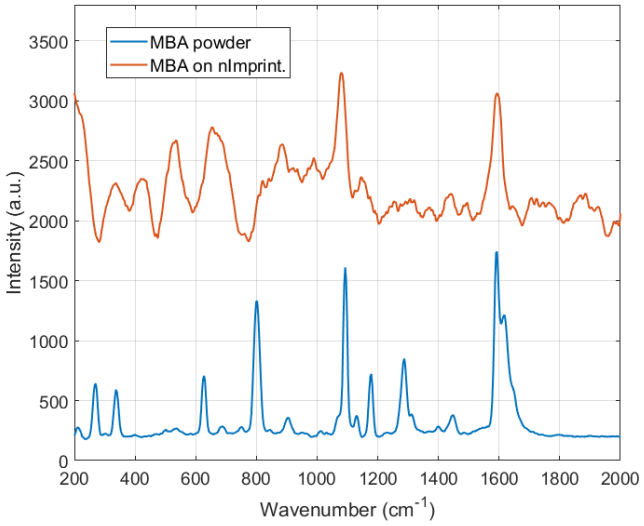

Figure 43: Spectrum of MBA on nanoimprinting sample. The acquisition is done with the 632nm laser with 10% of the power and 20 s of acquisition.

Using the data of the size got by the AFM images, the gold percentage is computed to be 32% of the total area of the sample and using the previously presented formula the enhancement is:

$$G \sim 6 \cdot 10^4 \tag{82}$$

Despite their theoretical good behavior due to the nice structures, these substrate have shown an almost inexistent enhancement for proteins measurement and a bad behavior in terms of spectrum, as it's possible to see from figure 43.
Proteins are much more fragile than molecules and this could be a reason why they were no success with these samples. However it is not completely understood why these substrate do not demonstrate a good behavior; the reasons still needs to be understood.

Anyway these kind of samples can still be used for a very useful purpose: we can exploit them as resonance sensor, that means looking at the plasmon resonance shift in order to understand if any changes happen on the surface.
They are really good for this measurement due to the nice and clear plasmon curve that can be obtained.

4.3.2 Klarite© surfaces

The second possibility is a commercial substrate composed by a gold surface with array of cavities with a pyramidal shape.
This substrate is not characterized by localized surface plasmons due to the continuous presence of a gold layer, but the idea is to create a reproducible and ordered rough surface that presents an enhancement due to propagating surface plasmons and hot spots of electromagnetic field. In fact SERS effect was at the beginning discovered dealing with rough metal surfaces that were exhibiting high enhancement of signal.

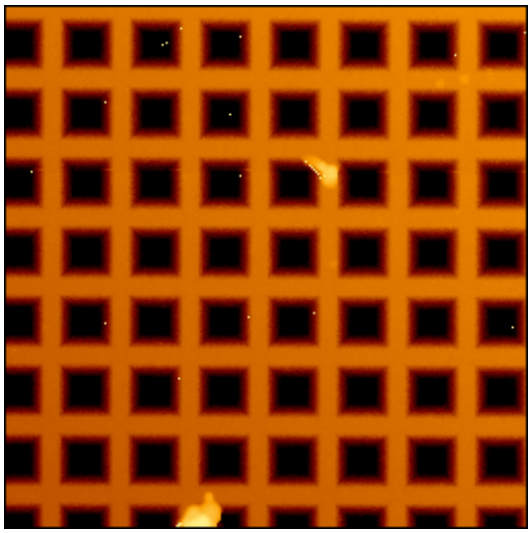

Figure 44: 15µm x 15µm AFM image of the klarite surface.

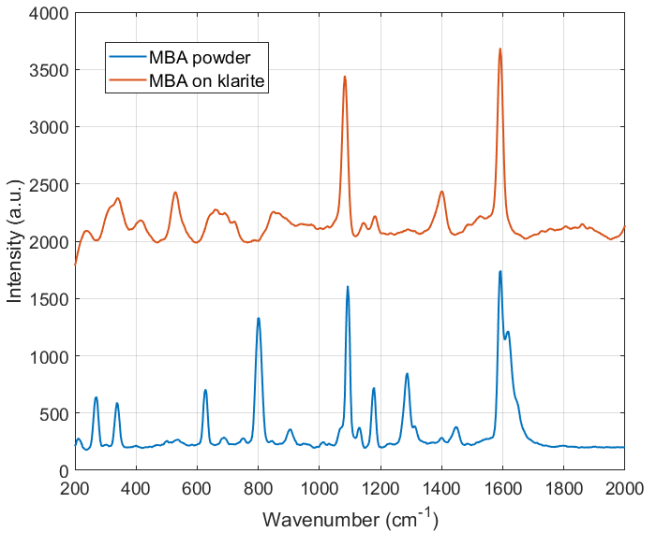

Figure 45: Spectrum of MBA on klarite sample. The acquisition is done with the 632nm laser with 10% of the power and 50 s of acquisition.

For the enhancement factor, we consider the surface fully covered by the gold, so the 100%. The obtained value is:

$$G \sim 1 \cdot 10^5 \tag{83}$$

For our purpose this sample seems to work quite well, the main drawback is that they cannot be produced by ourselves.
Moreover the cannot be used for the plasmon because this kind of substrates exploits the plasmons propagating at the interface, so they are not characterized by a single frequency resonance.

4.3.3 Gold nanoparticles

The last sample is the one got with the deposition of gold nanoparticles on glass slides (see Methodology chapter).
Looking with the AFM (figure 46) the final size of the nanoparticles seems to be around 60 nm, but in this case the convolution with the tip cannot be ignored. So looking at their height we can guess that the particles diameter is in the range between 50-60nm.

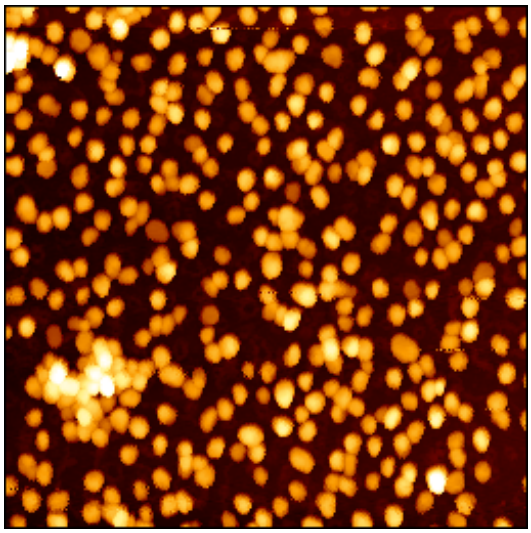

Figure 46: 2µm x 2µm AFM image of the nanoparticles

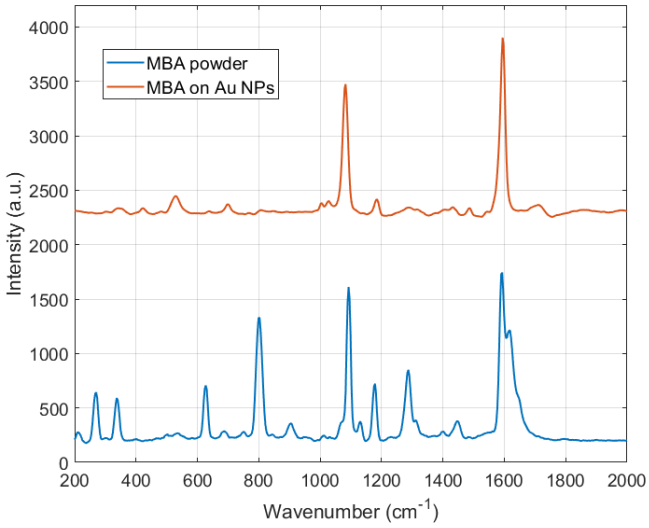

Figure 47: Spectrum of MBA on Au NPs. The acquisition is done with the 632nm laser with 10% of the power and 50 s of acquisition.

As it's possible to see from figure 47 the found spectrum is really well defined.
The gold surface is about 23% of the total area, leading to a final value of:

$$G \sim 3 \cdot 10^6 \tag{84}$$

So this kind of sample is working really well, they are often used for testing purpose because they can be easily prepared and they are not expensive.
The negative point could be that the particles are not always uniformly distributed on the surface and there can be some hotspot due to the vicinity of the particles that cannot be controlled (see figure 46). Statistically speaking, the collection area is around 150 µm^2, so in the investigated area there should be parts with less nanoparticles and parts with agglomerations, leading to a consistent result in different points.
About the plasmon resonance, this kind of samples are not the best solution because the curve is quite noisy and not very precise.

Enhancement Factors Here are summarized the final enhancement factors for the three samples.
It should be mentioned that the spectra are always taken in more points and then averaged in order to get the most precise and consistent result.

Sample	Enhancement Factor
nImprinting	$6 \cdot 10^4$
Klarite	$1 \cdot 10^5$
Au NPs	$3 \cdot 10^6$

Table 3: Temperature dependence on Integrated Intensity

After this analysis the final choice was oriented towards the klarite and the gold nanoparticles samples.
The nanocylinders showed basically no working in terms of spectra, especially with the proteins, while the other two samples were working well. The advantage of the nanoparticles is their cheap and easy fabrication that could be done more times in our laboratory.
Anyway the gold nanoimprinted nanocylinders showed a nice plasmon resonance, permitting to exploit them as a resonance sensor.

4.4 SERS of Proteins

4.4.1 BSA

Due to the easier incubation process previously explained, BSA is the first investigated protein. The steps are the ones explained in the methology, so for the BSA it consists in just putting the sample incubating in the solution.
A huge number of trials has been carried out with the nanoimprinted sample, unfortunately without getting any results concerning the spectrum, so here first are presented the data coming from the analysis of the plasmon resonance shift with this kind of sample.
These plots are useful to detect any changes on the surface of the sample, anyway this technique cannot be used as a qualitative detection.
For the analysis of the plasmon absorbance the peaks are fitted and the maximum is extracted from each curve in order to get the resonant wavelength.

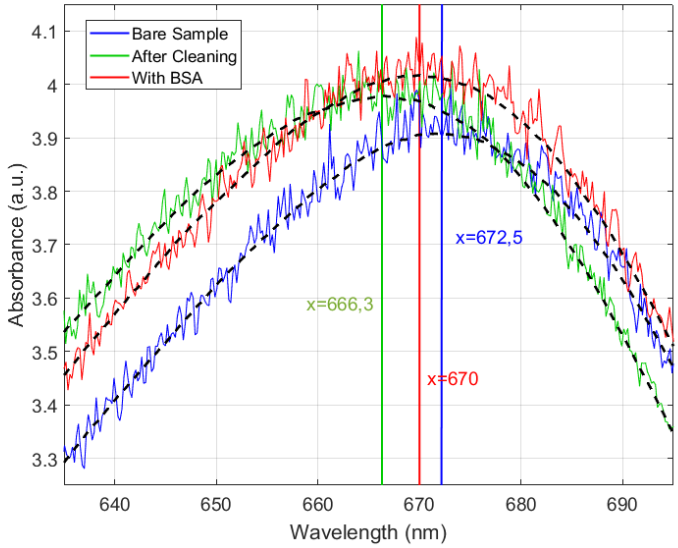

Figure 48: Plasmon resonances of the nanoimprinted sample referred to: bare sample, sample after UV-ozone cleaning, sample after incubation in the BSA solution.

Looking at the figure 48 it's possible to appreciate the shift in the resonant wavelength due to some variations on the sample's surface.
In particular the first step is the cleaning with the UV ozone machine: this process is one of the most used in research and it involves a photochemical reaction on the surface of the sample.
During the UV irradiation, the oxygen O_2 is dissociated in triplet atomic oxygen that will further combine with O_2 creating ozone O_3; when this kind of process is done a redshift of the plasmon resonance can be appreciated.
Finally after the incubation of the BSA the resonance undergoes a blueshift towards higher wavelengths, meaning that something has been added on the surface, BSA in this case. This can be seen as the proof of the proteins presence on the sample.

Here are presented the spectra got from the klarite and the gold nanoparticles samples with the relative acquisition parameters.
They are compared with the referent spectrum taken from the solution in order to evidence the

presence of BSA.
Please notice that all the graph are normalized in terms of laser power, numerical aperture, objective magnification and time exposure. Afterwards they are shifted up for a better visualization.

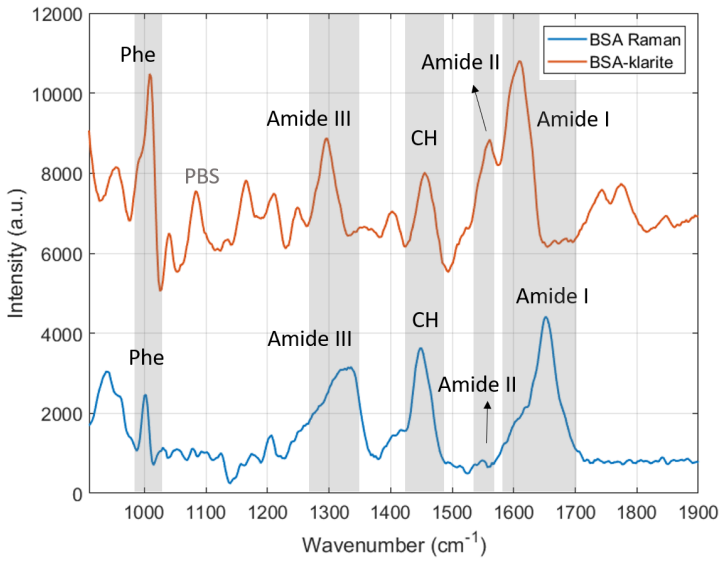

Figure 49: Comparison between 1mM of BSA in solution and 1mM deposited on the klarite surface.

The acquisition parameters related to figure 49 are:

- for the Raman solution: 785 nm Laser, 80x objective (NA 0.75), 100% power, 100s;
- for the SERS: 785 nm Laser, 80x objective (NA 0.75), 25% power, 80s.

From the two spectra is clearly appreciable the presence of BSA. There are some differences in the spectra that are related to the different conditions and environment around the BSA: in the first time the BSA is dispersed in solution, in the second is attached on the gold and this variation can be appreciated with a shift of the Amide I peak.
The presence of that band is the proof that the protein is still "alive" on the sample and in a detectable configuration.
Then it's possible to appreciate the appearance of the Amide II peak, characterized by a very poor intensity in the solution spectrum.

For the Gold Nanoparticles substrate:

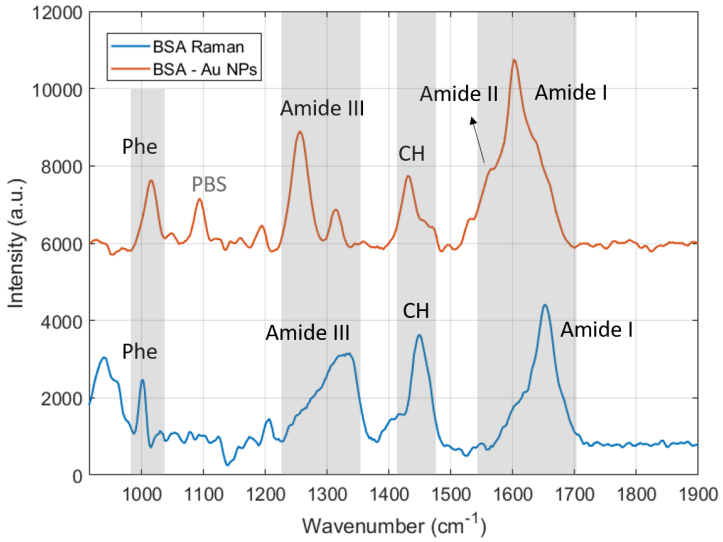

Figure 50: Comparison between 1mM of BSA in solution and 1mM deposited on the gold nanoparticles.

The acquisition parameters related to figure 50 are:

- for the Raman solution: 785 nm Laser, 80x objective (NA 0.75), 100% power, 100s;
- for the SERS: 632 nm Laser, 100x objective (NA 0.90), 10% power, 100s.

Also in this case we can see the presence of the protein as previously and the Amide I peak shifted about 50 cm^{-1}.
What it's interesting is looking at the Amide III complex that is related to the secondary structure of the protein. It is located between 1200 and 1350 cm^{-1} and the relative intensities of its peaks are changing varying the configuration of the protein.

Then looking at the spectra we can observe that they are always different if taken in different conditions because the spectrum depends on the proteins configuration and how it's interacting with the surroundings.
Even for the two SERS spectra there are still some big difference, in particular what is changing is the relative intensity of the Amide III (around 1300 cm^{-1}).

We can summarize here the main differences between the two SERS sample:

- klarite samples are not characterized by localized surface plasmons due to the continuous layer of gold, in their case we deal with with propagating surface plasmons. Differently for gold nanoparticles we are have the localization of the effect;
- the spectra are taken with two different wavelength lasers;
- for klarite the acquisition is done in air, so the sample is dried; differently, for the gold NPs, the only way to catch the the BSA was to acquire in liquid. SERS spectra of proteins are really modified by the local environment;
- BSA links differently on a substrate completely covered by gold with respect to gold nanoparticles.

Considering these facts, differences in the spectra are justified and moreover they could be useful for further studies about the conformation of the proteins structure.
In our case what is important is to detect the BSA, so be able to see its presence. As a reference we can use the Amide I peak, whose intensity will give informations about the presence and the concentration of the protein.

4.4.2 Lysozyme

In the case of lyzozyme, the followed process is the surface functionalization explained in the methodology chapter.
Also in this case a study of the plasmon resonance shift has been carried out with the nanoimprinting sample in order to verify the working of the surface functionalization.
So the plasmon has been acquired in 4 different moments: the bare sample, after the UV-ozone cleaning, after the surface functionalization process with aptamer and MOH and finally after the incubation in the lysozyme solution.

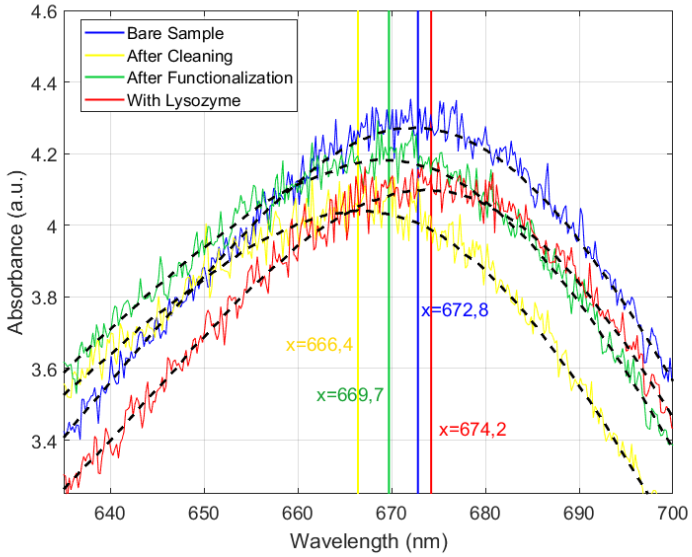

Figure 51: Plasmon resonances of the nanoimprinted sample referred to: bare sample, sample after UV-ozone cleaning, sample after surface functionalization, after lysozyme incubation.

Looking at figure 51 we can see that at each step there are changes on the surface compositions.
As previously the cleaning causes a redshift in the resonance while adding molecules on the surface (functionalization) we perform a blueshift.
The last blueshift shows clearly the presence of new stuff on the surface, lysozyme in this case.

After each step a SERS spectrum is acquired in order to look at the differences in composition, here are shown the different moments of the process:

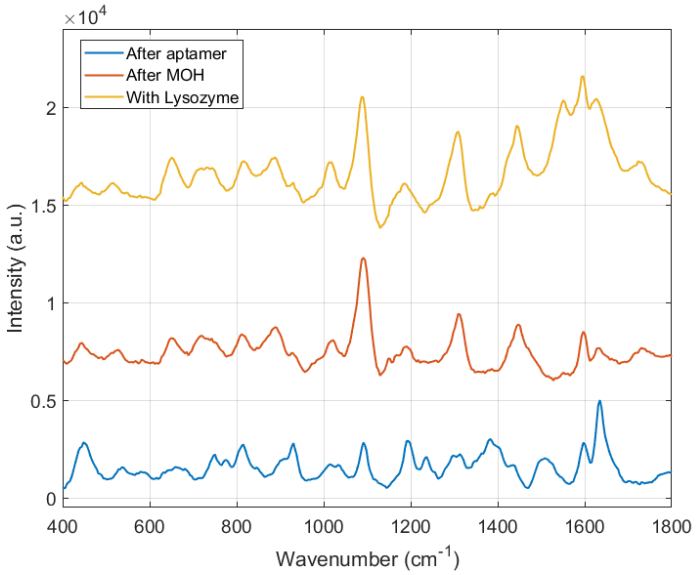

Figure 52: SERS spectra taken from the gold nanoparticles in different steps. The acquisition parameters are: laser 660nm, power 10%, acquisition time 20 s and the used lens is the 80x.

Looking at th figure 52 it's possible to extract some considerations:

- the aptamer spectrum is not so well defined, in fact, changing the acquisition point, the spectrum will be affected by some differences. This because without the blocking molecule the aptamer can arrange in a lot of different configurations leading to variations in the spectra;
- after putting the MOH, the spectrum becomes much more stable and consistent in different areas of the sample, leading to a reproducible result for further comparison;
- after adding the lysozyme there are some changes in the spectrum, especially a big contribution in the area around 1600 cm^{-1} that is the zone typical of the Amide I peak.

In order to investigate the presence of lysozyme we can plot together the two spectra (after the functionalization process and with lysozyme) and compare them with the reference Raman spectrum for the protein in solution.

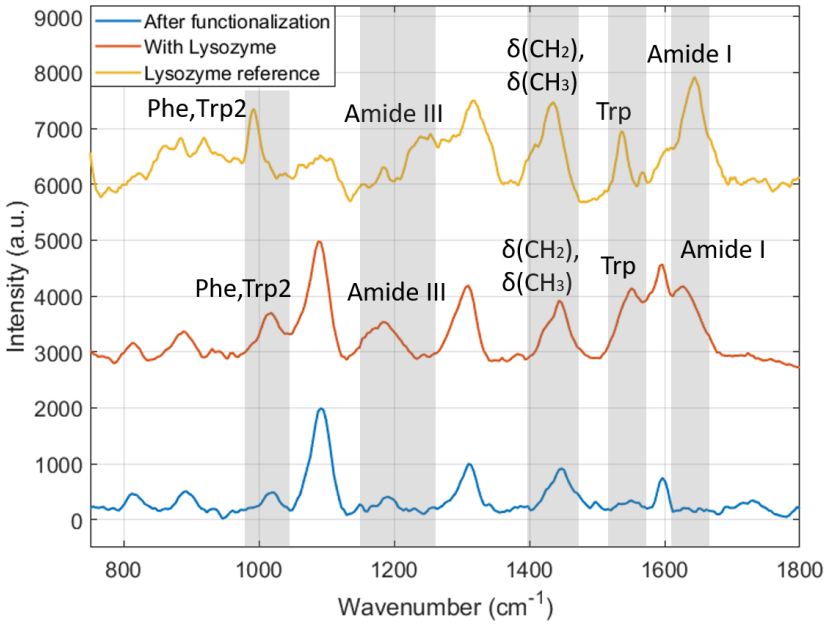

Figure 53: Comparison between the SERS spectra from Au NPs and the reference one in solution. The acquisition parameters for the SERS are: laser 660nm, power 10%, acquisition time 20 s. For the Raman solution: 785nm, power 100%, 225 s.

From the figure 53 we can notice that the differences between the blue (after MOH) and the red (after lyzozyme) correspond to the reference peaks of the protein.
The most clear result is the contribution at the Amide I peak around 1630 cm^{-1} and from the tryptophan vibration at 1550 cm^{-1}; then other changes in the spectra can be noticed but less evidently due to superimposition of some peaks with the aptamer ones.
So the information related to the concentration can be got from the peaks at 1550 and 1630 cm^{-1}, first fitting the shape of the peak and then integrating to get the intensity and so an estimation of the amount of protein on the sample.

5 Conclusions & Outlooks

The work done was divided into two parallel parts, one related to the biosensor for proteins and the other concerning the membrane.

For the sensing, three kinds of sample are analyzed: the imprinted nanocylinders, the gold surfaces with pyramidal cavities and the gold nanoparticles.
The best device found in term of spectrum both for MBA and proteins is the sample with Gold nanoparticles, whose advantages are that is home-made and its low cost.
Anyway the nanoimprinting sample has been a lot exploited as a resonance sensor to detect variations on the surface of the sample.

With the nanoparticles sample we managed to catch the BSA simply incubating the sample in the solution while for the lysozyme a functionalization with the aptamer was needed, leading to the detection of the protein.
We can here summarize the possible ways to detect a protein related to the concentration:

- AFM: for concentration lower than 200 nM, this technique can be used for a quantitative measurement;
- SERS with AuNPs: for concentration until few µM, below this it begins to be difficult and not very consistent;
- Raman on solution: for concentration higher than 0.5 mM.

Referring to the spectra, informations related to the amount of proteins could be got integrating the Amide I peak around 1630 cm^{-1}, that gives information about the basic structure of the protein, i.e. its presence and concentration.

Concerning the membrane, the first part of the work was devoted to the building of the device and a theoretical analysis has been carried out in order to try to understand how the ions behave in such a system.
For the electrical characterization, a rectification has been found in the I-V curves of the charged polymer and we showed that it was coming from an entropic effect performing a study in temperature.
This effect is given by the conical shape of the nanopores that can give a not negligible energy contribution, leading to a smart way to evidence the entropy in isolated system; generalizing this phenomenon can be used in variegated way to control the transport at the nano and micro scale and it can be exploited in different ways for different purposes.

The next step would be to characterize the ability of the system to pump ions and molecules on one compartment and so to increase their concentrations.
In order to verify the working of the pumping, the SERS sensor can be used to be able to appreciate small variations of concentration. A very useful step should be to use a more stable membrane, polyimide for example, because we noticed that after some trials the membrane was loosing its working principle. Moreover polyimide is neutral, avoiding any electrostatic effect between the ions and the membrane.

More generally, we analyzed two different way that can be exploited together to get in the best case an high-sensitivity molecular sensor.
What is interesting is the completely different background coming from these two subjects:

concerning the SERS biosensor, it's a pretty physical phenomenon applied to biology, in the case of the membrane we deal with pure biophysics.

6 Bibliography

1. Bhalla N, Jolly P, Formisano N, Estrela P. **Introduction to biosensors.** Essays Biochem. 2016 Jun 30;60(1):1-8. doi: 10.1042/EBC20150001.
2. Anthony P.F. Turner, Isao Karube, George S. Wilson **Biosensors: Fundamentals and Applications.** Oxford University Press.
3. Mehrotra P. **Biosensors and their applications - A review.** J Oral Biol Craniofac Res. 2016 May-Aug;6(2):153-9. doi: 10.1016/j.jobcr.2015.12.002.
4. Tuan Vo-Dinh, **SERS chemical sensors and biosensors: new tools for environmental and biological analysis.** Sensors and Actuators B: Chemical, Volume 29, Issues 1-3, 1995, Pages 183-189, ISSN 0925-4005, https://doi.org/10.1016/0925-4005(95)01681-3.
5. Bantz KC, Meyer AF, Wittenberg NJ, Im H, Kurtulus O, Lee SH, Lindquist NC, Oh SH, Haynes CL. **Recent progress in SERS biosensing.** Phys Chem Chem Phys. 2011 Jun 28;13(24):11551-67. doi: 10.1039/c0cp01841d.
6. https://en.wikipedia.org/wiki/Spectroscopy.
7. Wallace MB, Wax A, Roberts DN, Graf RN. **Reflectance spectroscopy.** Gastrointest Endosc Clin N Am. 2009 Apr;19(2):233-42. doi: 10.1016/j.giec.2009.02.008.
8. Nilapwar SM, Nardelli M, Westerhoff HV, Verma M. **Absorption spectroscopy.** Methods Enzymol. 2011;500:59-75. doi: 10.1016/B978-0-12-385118-5.00004-9.
9. Liu KL. **[Review of atomic spectroscopy].** Guang Pu Xue Yu Guang Pu Fen Xi. 2005 Jan;25(1):95-103. Review. Chinese.
10. Pänke O, Balkenhohl T, Kafka J, Schäfer D, Lisdat F. **Impedance spectroscopy and biosensing.** Adv Biochem Eng Biotechnol. 2008;109:195-237.
11. Mathew NA, Yurs LA, Block SB, Pakoulev AV, Kornau KM, Wright JC. **Multiple quantum coherence spectroscopy.** J Phys Chem A. 2009 Aug 20;113(33):9261-5. doi: 10.1021/jp903337s.
12. Raman, C. V. (1928). **A new radiation.** Indian J. Phys. 2: 387-398.
13. http://en.wikipedia.org/wiki/Raman_spectroscopy.
14. **Physical and Theoretical Chemistry Textbook/Spectroscopy/Vibrational Spectroscopy/ Raman Spectroscopy/Raman Theory.** Website: https://chem.libretexts.org/Textbook_Maps/Physical_and_Theoretical_Chemistry_Textbook_Maps/Supplemental_Modules_(Physical_and_Theoretical_Chemistry)/Spectroscopy/Vibrational_Spectroscopy/Raman_Spectroscopy/Raman%3A_Theory.
15. Szymanski, H. A.,**Raman Spectroscopy: Theory and Practice.** Plenum Press, New York, 1967.
16. McCreery, R. L., **Raman Spectroscopy for Chemical Analysis.** John Wiley & Sons, Inc., New York, 2000.
17. Stencel, J. M.**Raman Spectroscopy for Catalysis.** Van Nostrand Reinhold, New York, 1990.
18. Grasselli, J. G.; Bulkin, B. J. **Analytical Raman Spectroscopy.** John Wiley & Sons, Inc., New York, 1991.
19. Harris, D. C.; Bertolucci, M. D.; **Symmetry and Spectroscopy: an introduction to vibrational and electronic spectroscopy.** Dover Publications, Inc., New York, 1989.
20. McQuarrie, D. A., Simon, J.D., **Physical Chemistry: A Molecular Approach.** University Science Books, Sausalito, California, 1997; 518-521.
21. **Physical and Theoretical Chemistry Textbook/Spectroscopy/Vibrational Spectroscopy/ Raman Spectroscopy/Raman Theory.** Website: https://chem.libretexts.org/Textbook_Maps/Physical_and_Theoretical_Chemistry_Textbook_Maps/Supplemental_Modules_(Physical_and_Theoretical_Chemistry)/Spectroscopy/Vibrational_Spectroscopy/Vibrational_Modes/Normal_Modes.
22. Housecroft, C.E., Sharpe, A.G., **Inorganic Chemistry.** Pearson Education Limited, England, 2008, 107.
23. Jiang N, Zhuo X, Wang J. **Active Plasmonics: Principles, Structures, and Applications.** Chem Rev. 2018 Mar 28;118(6):3054-3099. doi: 10.1021/acs.chemrev.7b00252
24. Lee JH, Cho HY, Choi HK, Lee JY, Choi JW. **Application of Gold Nanoparticle to Plasmonic Biosensors.** Int J Mol Sci. 2018 Jul 11;19(7). pii: E2021. doi: 10.3390/ijms19072021.
25. Yonzon CR, Jeoung E, Zou S, Schatz GC, Mrksich M, Van Duyne RP. **A comparative analysis of localized and propagating surface plasmon resonance sensors: the binding of concanavalin a to a monosaccharide functionalized self-assembled monolayer.** J Am Chem Soc. 2004 Oct 6;126(39):12669-76.
26. Book by Marc Lamy de la Chapelle, Annemarie Pucci, **Nanoantenna: Plasmon-Enhanced Spectroscopies for Biotechnological Applications.** January 24, 2013 by Pan Stanford.
27. **"Nanothermics"** course notes, Bruno Palpant.
28. Fleischmann, M.; PJ Hendra & AJ McQuillan (15 May 1974). **Raman Spectra of Pyridine Adsorbed at a Silver Electrode.** Chemical Physics Letters. 26 (2): 163-166. doi:10.1016/0009-2614(74)85388-1.
29. Ding SY, You EM, Tian ZQ, Moskovits M. **Electromagnetic theories of surface-enhanced Raman spectroscopy.** Chem Soc Rev. 2017 Jul 7;46(13):4042-4076.
30. Morton SM, Jensen L. **Understanding the molecule-surface chemical coupling in SERS.** J Am Chem Soc.

2009 Mar 25;131(11):4090-8.
31. Pablo G. Etchegoin and Eric C. Le Ru, **Basic Electromagnetic Theory of SERS**. From *Surface Enhanced Raman Spectroscopy: Analytical, Biophysical and Life Science Applications.* Edited by Sebastian Schlucker.
32. R. Ruppin, **Electric field enhancement near a surface bump.** Solid State Communications, Volume 39, Issue 8, 1981, Pages 903-906, ISSN 0038-1098, https://doi.org/10.1016/0038-1098(81)90034-X.
33. Le Ru, Eric & Blackie, EJ & Meyer, M & Etchegoin, P.G.. (2007). **Surface Enhanced Raman Scattering Enhancement Factors: A Comprehensive Study.** Journal of Physical Chemistry C - J PHYS CHEM C. 111. 10.1021/jp0687908.
34. Kneipp, Katrin & Wang, Yang & Kneipp, Harald & T. Perelman, Lev & Itzkan, Irving & Dasari, Rakesh & S. Feld, Michael. (1997).**Single Molecule Detection Using Surface-enhanced Raman Scattering (SERS).** Physical Review Letters. 78. 1667. 10.1103/PhysRevLett.78.1667.
35. Liu, Hongwen & Zhang, Ling & Lang, Xing & Yamaguchi, Yoshinori & Iwasaki, Hiroshi & Inouye, Yasushi & Xue, Qikun & Chen, Mingwei. (2011). **Single molecule detection from a large-scale SERS-active Au.** Scientific reports. 1. 112. 10.1038/srep00112.
36. Lennart Sjögren, **Lecture notes Stochastic processes.** Chapter 6: *Brownian Motion: Langevin Equation*.
37. Gerhard Schmid, P. Sekhar Burada, Peter Talkner, and Peter Hänggi, **Rectification Through Entropic Barriers.** Department of Physics, University of Augsburg, Universitätsstr. 1, 86135, Augsburg, Germany.
38. R. D. Astumian and M. Bier. **Fluctuation driven ratchets: molecular motors.** Phys. Rev. Lett. 72, 1766 (1994)
39. Lairez D, Clochard M-C, Wegrowe J-E. **The concept of entropic rectifier facing experiments.** Scientific Reports. 2016;6:38966. doi:10.1038/srep38966.
40. Hanggi, Peter & Marchesoni, Fabio. (2008). **Artificial Brownian motors: Controlling transport on the nanoscale.** Review of Modern Physics. 81. 10.1103/RevModPhys.81.387.
41. I. D. Kosinska, I. Goychuk, M. Kostur, G. Schmid, and P. Hanggi. **Rectification in synthetic conical nanopores: a one-dimensional Poisson-Nernst-Planck model.** Phys. Rev. E, 77, 031131 (2008)
42. C. Malmberg and A. Maryott, **Dielectric constant of water from 0° to 100°C.** J. Res. Nut. Bureau of Stanah&, vol. 56, pp. 1-8, 1956.
43. https://en.wikipedia.org/wiki/Protein.
44. https://en.wikipedia.org/wiki/Bovine_serum_albumin.
45. Moriyama Y, Watanabe E, Kobayashi K, Harano H, Inui E, Takeda K. **Secondary structural change of bovine serum albumin in thermal denaturation up to 130 degrees C and protective effect of sodium dodecyl sulfate on the change.**J Phys Chem B. 2008 Dec 25;112(51):16585-9. doi: 10.1021/jp8067624. PubMed PMID:19367984.
46. Debasmita Ghosh, Somrita Mondal, Srabanti Ghosha and Abhijit Saha **Protein conformation driven biomimetic synthesis of semiconductor nanoparticles** Journal of Materials Chemistry. DOI: 10.1039/C1JM13730A J. Mater. Chem., 2012,22, 699-706.
47. Lu R, Li WW, Katzir A, Raichlin Y, Yu HQ, Mizaikoff B. **Probing the secondary structure of bovine serum albumin during heat-induced denaturation using mid-infrared fiberoptic sensors.** Analyst. 2015 Feb 7;140(3):765-70. doi: 10.1039/c4an01495b. PubMed PMID: 25525641.
48. Givens BE, Xu Z, Fiegel J, Grassian VH.**Bovine serum albumin adsorption on SiO(2) and TiO(2) nanoparticle surfaces at circumneutral and acidic pH: A tale of two nano-bio surface interactions.** J Colloid Interface Sci.2017 May 1;493:334-341. doi:10.1016/j.jcis.2017.01.011.
49. Fazio, Barbara & Foti, Antonino & Messina, Elena & Irrera, Alessia & Grazia Donato, Maria & Villari, Valentina & Micali, Norberto & Marago, Onofrio M. & Gucciardi, P. (2016). **SERS detection of Biomolecules at Physiological pH via aggregation of Gold Nanorods mediated by Optical Forces and Plasmonic Heating** OPEN. Scientific Reports. 6. 26952. 10.1038/srep26952.
50. website of Biological Magnetic Resonance Data Bankhttp://www.bmrb.wisc.edu.
51. https://en.wikipedia.org/wiki/Lysozyme.
52. http://www.npl.co.uk/science-technology/surface-and-nanoanalysis/surface-and-nano-analysis-basics/introduction-to-afm-atomic-force-microscopy.
53. Trache A, Meininger GA. **Atomic force microscopy (AFM).** Curr Protoc Microbiol. 2008 Feb;Chapter 2:Unit 2C.2. doi: 10.1002/9780471729259.mc02c02s8.
54. https://www.jpk.com/products/atomic-force-microscopy/qi-mode.
55. David C, Guillot N, Shen H, Toury T, de la Chapelle ML. **SERS detection of biomolecules using lithographed nanoparticles towards a reproducible SERS biosensor.** Nanotechnology. 2010 Nov 26;21(47):475501. doi: 10.1088/0957-4484/21/47/475501.
56. Maximilien Cottat, Cristiano D'Andrea, Ryohei Yasukuni, Natalia Malashikhina, Ruta Grinyte, Nathalie Lidgi-Guigui, Barbara Fazio, Angela Sutton, Olivier Oudar, Nathalie Charnaux, Valery Pavlov, Andrea

Toma, Enzo Di Fabrizio, Pietro G. Gucciardi, and Marc Lamy de la Chapelle. **High Sensitivity, High Selectivity SERS Detection of MnSOD Using Optical Nanoantennas Functionalized with Aptamers.** The Journal of Physical Chemistry C 2015 119 (27), 15532-15540 DOI: 10.1021/acs.jpcc.5b03681

57. Thioune, Néné & Lidgi-Guigui, Nathalie & Cottat, Maximilien & Gabudean, Ana Maria & FOCSAN, Monica & Benoist, Henri & Astilean, Simion & Lamy de la Chapelle, Marc. (2013). **Study of gold nanorods-protein interaction by localized surface plasmon resonance spectroscopy.** Gold bulletin. 46. 275-281. 10.1007/s13404-013-0118-5.
58. Patrick N. Sisco and Catherine J. Murphy. **Surface-Coverage Dependence of Surface-Enhanced Raman Scattering from Gold Nanocubes on Self-Assembled Monolayers of Analyte.** The Journal of Physical Chemistry A 2009 113 (16), 3973-3978 DOI: 10.1021/jp810329j
59. Gokhale, Ankush & Lu, Jue & Lee, Ilsoon. (2013). **Recent Progress in the Development of Novel Nanostructured Biosensors for Detection of Waterborne Contaminants.** 19. 1-34. 10.1007/978-3-319-02772-2_1.
60. Zhang, Dongmao & Ansar, Siyam & Vangala, Karthikeshwar & Jiang, Dongping. (2010). **Protein adsorption drastically reduces surface-enhanced Raman signal of dye molecules.** Journal of Raman Spectroscopy. 41. 952 - 957. 10.1002/jrs.2548.
61. Zhang J, Liu B, Liu H, Zhang X, Tan W. **Aptamer-conjugated gold nanoparticles for bioanalysis.** Nanomedicine (Lond). 2013 un;8(6):983-93. doi: 10.2217/nnm.13.80. Review.
62. Loredana Florina Leopold, István Szabolcs Tódor, Zorita Diaconeasa, Dumitrita Rugina, Andrei Stefancu, Nicolae Leopold, Cristina Coman. **Assessment of PEG and BSA-PEG gold nanoparticles cellular interaction.** Colloids and Surfaces A: Physicochemical and Engineering Aspects, Volume 532, 2017, Pages 70-76, ISSN 0927-7757, https://doi.org/10.1016/j.colsurfa.2017.06.061.
63. Xiao-Shan Zheng, Pei Hu, Yan Cui, Cheng Zong, Jia-Min Feng, Xin Wang, and Bin Ren. **BSA-Coated Nanoparticles for Improved SERS-Based Intracellular pH Sensing.** Analytical Chemistry 2014 86 (24), 12250-12257. DOI: 10.1021/ac503404u
64. Albrecht, M. Grant; J. Alan Creighton (1977). **Anomalously Intense Raman Spectra of Pyridine at a Silver Electrode.** Journal of the American Chemical Society. 99 (15): 5215-5217. doi:10.1021/ja00457a071.
65. Gao W, Li B, Yao R, Li Z, Wang X, Dong X, Qu H, Li Q, Li N, Chi H, Zhou B, Xia Z. **Intuitive Label-Free SERS Detection of Bacteria Using Aptamer-Based in Situ Silver Nanoparticles Synthesis.** Anal Chem. 2017 Sep 19; doi: 10.1021/acs.analchem.7b01813.
66. Boushell, V. , Pang, S. and He, L. (2017). **Aptamer-Based SERS Detection of Lysozyme on a Food-Handling Surface.** Journal of Food Science, 82: 225-231. doi:10.1111/1750-3841.13582
67. Xing L, Lin K, Zhou X, Liu S, Luo Y. **Multistate Mechanism of Lysozyme Denaturation through Synchronous Analysis of Raman Spectra.** J Phys Chem B. 2016 Oct 10.
68. Yang L, Fu C, Wang H, Xu S, Xu W. **Aptamer-based surface-enhanced Raman scattering (SERS) sensor for thrombin based on supramolecular recognition, oriented assembly, and local field coupling.** Anal Bioanal Chem. 2017 Jan;409(1):235-242. doi: 10.1007/s00216-016-9992-z.
69. I. D. Kosinska, I. Goychuk, M. Kostur, G. Schmid, and P. Hanggi. **Rectification in synthetic conical nanopores: a one-dimensional Poisson-Nernst-Planck model.** Phys. Rev. E, 77, 031131 (2008)
70. T.Y. Tsong and T.D. Xie. **Ion pump as molecular ratchet and effects of noise: electric activation of cation pumping by Na,K-ATPase.** Appl. Phys. A, 75, 345 (2002)